iScience

CellPress
OPEN ACCESS

Article

IGFBP2 derived from PO-MSCs promote epithelial barrier destruction by activating FAK signaling in nasal polyps

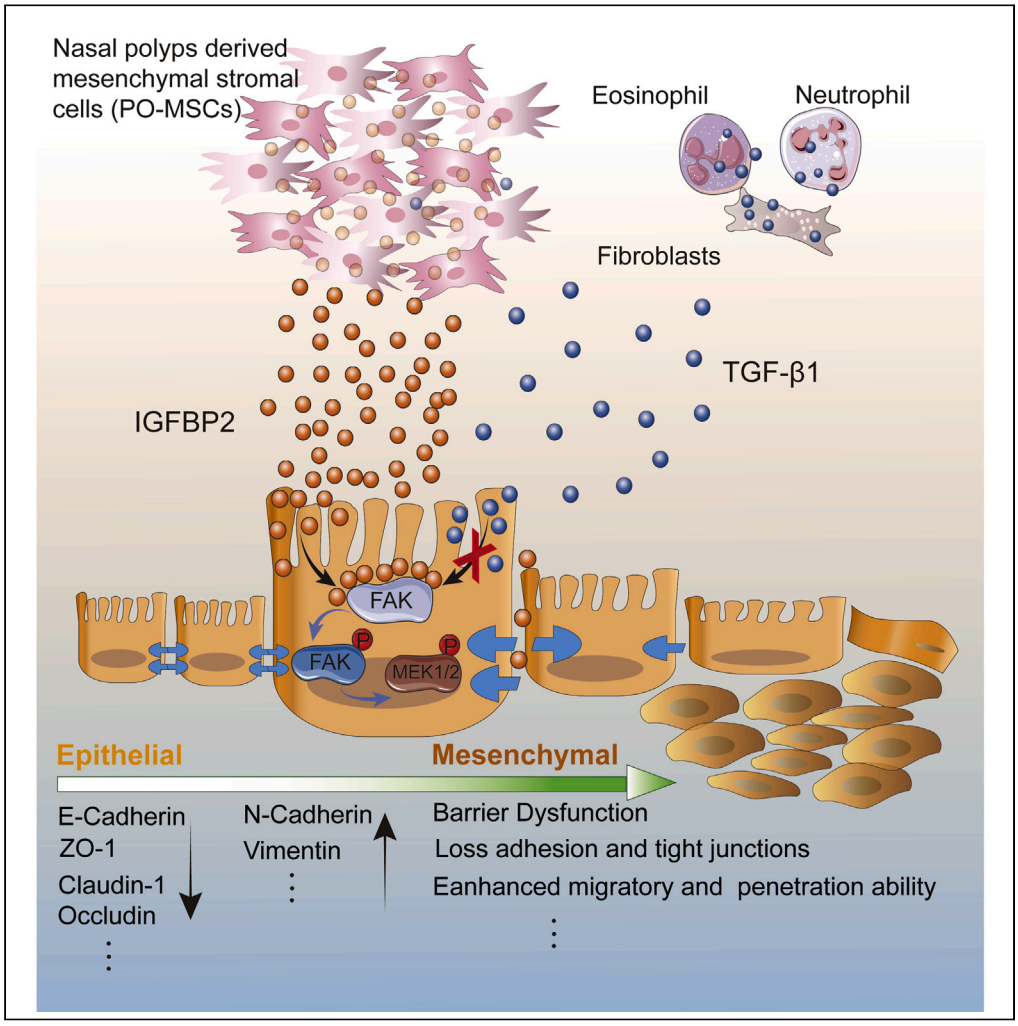

Bo You, Ting Zhang, Wei Zhang, ..., Zhifeng Gu, Lei Cheng, Jing Chen

chenjing0408@hotmail.com (J.C.)
chenglei@jsph.org.cn (L.C.)
guzf@ntu.edu.cn (Z.G.)

Highlights

Impairment of epithelial barrier function and enhancement of EMT in NPs

PO-MSCs promoted the EMT process and epithelial barrier dysfunction in NPs

IGFBP2, but not EVs, exhibited crucial role on EMT and epithelial barrier destruction

IGFBP2 mediated EMT and barrier destruction via activating the FAK signaling pathway

You et al., iScience 26, 106151
March 17, 2023
https://doi.org/10.1016/j.isci.2023.106151

iScience

CellPress
OPEN ACCESS

Article

IGFBP2 derived from PO-MSCs promote epithelial barrier destruction by activating FAK signaling in nasal polyps

Bo You,[1,2,6] Ting Zhang,[1,2,6] Wei Zhang,[1,2,6] Yinyin Pei,[1,2] Danyi Huang,[1,2] Yun Lei,[1,2] Shaocong Zhang,[1,2] Changyu Qiu,[3,4] Jie Zhang,[1,2] Zhifeng Gu,[5,7,*] Lei Cheng,[3,4,7,*] and Jing Chen[1,2,7,*]

SUMMARY

The nasal polyps (NPs) microenvironment comprises multiple cell types, including mesenchymal stromal cells (MSCs). Insulin-like growth factor binding protein 2 (IGFBP2) plays crucial roles in cell proliferation, differentiation and more. However, the role of NPs-derived MSCs (PO-MSCs) and IGFBP2 in NPs pathogenesis remains poorly defined. Herein, primary human nasal epithelial cells (pHNECs) and MSCs were extracted and cultured. Extracellular vesicles (EVs) and soluble proteins were isolated to investigate the role of PO-MSCs on epithelial-mesenchymal transition (EMT) and epithelial barrier function in NPs. Our data showed that IGFBP2, but not EVs from PO-MSCs (PO-MSCs-EVs), exhibited a crucial role in EMT and barrier destruction. Moreover, focal adhesion kinase (FAK) signaling pathway is necessary for IGFBP2 to exert its functions in human and mice nasal epithelial mucosa. Altogether, these findings may improve the current understanding of the role of PO-MSCs in NPs microenvironment and ultimately contribute to the prevention and treatment of NPs.

INTRODUCTION

As a common, complex upper respiratory condition, chronic rhinosinusitis with nasal polyps (CRSwNPs) is a heterogeneous inflammatory disease of the sinuses and nasal mucosa, characterized by epithelial barrier destruction, increased permeability, tissue remodeling, and nasal polyps (NPs) formation.[1,2] The development of NPs indicates a refractory clinical phenotype, with severe symptoms and poor prognosis.[3,4] Loss of epithelial cells function and aberrant tight junctions (TJs) protein expression may mediate the destruction of the mucosal epithelial barrier and host defense in NPs.[4–6] Despite extensive studies, the roles of local microenvironmental elements such as mesenchymal stromal cells (MSCs) in NPs remain unclear.

MSCs are multipotent cells that can obtained from sources such as the umbilical cord, bone marrow, muscles, neural tissues, and adipose tissues, including NPs.[7,8] Owing to their multi-differentiation potential, heterogeneity and immunogenicity, MSCs have attracted much attention in recent years.[9] Previous studies have shown that MSCs provide promising evidence for the elucidation of the pathogenesis of NPs and the development of new therapeutic strategies due to their immunomodulatory properties.[10] Of interest, NPs derived MSCs (PO-MSCs) can be distinguished from those isolated from healthy inferior turbinate tissues and may participate in NPs pathogenesis.[11] In addition, the proliferation and growth capacity of PO-MSCs are significantly decreased, leading to intractable and aberrant NPs remodeling.[12] In 2007, Gregorio et al. isolated PO-MSCs from various cells in the microenvironment of NPs tissue.[8] These cells, designated PO-MSCs, showed normal morphology and differentiation potential. However, immunophenotyping demonstrated a deficiency in immune-related molecules compared with that of bone marrow-derived MSCs (BM-MSCs) based on analyses of molecular characteristics and gene expression patterns. Importantly, Gene Ontology analysis showed that the differentially expressed genes were associated with epithelial and matrix remodeling in PO-MSCs, which may be linked to NPs pathogenesis.[8] Notably, disruption of homeostasis among the abnormal differentiation of PO-MSCs, decreased proliferation of nasal epithelial cells, and the epithelial-mesenchymal transition (EMT) was shown to be closely correlated with the cellular pathogenesis of NPs.[13] Although EMT and epithelial barrier destruction are known to affect the NPs persistent aberrant microenvironment and tissue remodeling,[14–17] the potential functions of PO-MSCs have not been fully elucidated.

[1]Institute of Otolaryngology Head and Neck Surgery, Affiliated Hospital of Nantong University, Nantong 226001, China

[2]Department of Otolaryngology Head and Neck Surgery, Affiliated Hospital of Nantong University, Nantong 226001, China

[3]Department of Otorhinolaryngology & Clinical Allergy Center, The First Affiliated Hospital, Nanjing Medical University, Nanjing 210029, China

[4]International Center for Allergy Research, Nanjing Medical University, Nanjing 210029, China

[5]Research Center of Clinical Medicine, Affiliated Hospital of Nantong University, Nantong 226001, China

[6]These authors contributed equally

[7]Lead contact

*Correspondence: chenjing0408@hotmail.com (J.C.), chenglei@jsph.org.cn (L.C.), guzf@ntu.edu.cn (Z.G.)

https://doi.org/10.1016/j.isci.2023.106151

Table 1. Patient characteristics

Characteristics	Controls	Patients with CRSwNP	p value
Total no. of patients	36	80	–
Tissue used	IT	NP	–
Sex, male, N (%)	20 (55.6)	44 (55)	0.956
Age (years), mean (SD)	41.75 (3.93)	43.3 (3.93)	0.052
Asthma, N (%)	0 (0)	5 (6.25)	0.322
Aspirin intolerance, N (%)	0 (0)	0 (0)	–
AR, N (%)	0 (0)	4 (5)	0.309
Lund-Mackay CT score, mean (SD)	0	13.21 (2.78)	–
Lund-Kennedy score, mean (SD)	0	6.08 (0.96)	–

NP, nasal polyps; IT, inferior turbinate; AR, allergic rhinitis; SD, SDp< 0.05 was considered statistically significant.

MSCs tend to be recruited by injured tissues, exerting both positive and negative effects on diseases.[9,18] MSCs regulate various diseases, mainly by secreting extracellular vesicles (EVs) or the secretome, i.e., growth factors, cytokines, and soluble proteins.[19–21] Insulin-like growth factor binding protein-2 (IGFBP2), as an abundant secreted protein, is a vital member of the IGFBP family, which exert functions either independently or through binding to IGF sites.[22] IGFBP2 overexpression promotes malignant biological behaviors by regulating the immune microenvironment, accelerating proliferation and differentiation, and stimulating angiogenesis and EMT in various cancers, including breast cancer,[23] pancreatic cancer[24], and hepatocellular carcinoma.[25] Furthermore, IGFBP2 secreted from MSCs activates inflammatory process and immune-related signaling pathways to regulate disease progression.[26] In view of MSCs contributing to aggressive phenotype of diseases, the present study was aimed to illustrate the role of PO-MSCs derived IGFBP2 in regulating epithelial barrier destruction in NPs. Focal adhesion kinase (FAK), a protein tyrosine kinase activated in several diseases, drives disease progression and deterioration.[27–29] As the core of the EMT phenotype, phosphorylation of FAK is often used as an indicator of pathology, regulating the EMT, migration, and stem cells through complex signaling networks.[30,31] Of interest, IGFBP2 is significantly associated with FAK phosphorylation,[32,33]further increasing our interest in the interaction between FAK and IGFBP2 in NPs microenvironment.

Accordingly, in this study, we evaluated the roles of PO-MSCs-derived IGFBP2 in regulating epithelial barrier destruction in NPs. We hypothesized that PO-MSCs may mediate the destruction of the epithelial barrier through protein secretion and signaling pathway activation in the local microenvironment, thereby contributing to NPs pathogenesis. We observed the aberrant epithelial barrier functions in NPs tissues and TGF-β1-induced pHNECs EMT model *in vitro*. We also determined that PO-MSCs could mediate the destruction of the epithelial barrier through the activation of FAK signaling pathway in NPs. Importantly, the soluble protein IGFBP2 in PO-MSCs conditioned medium (CM), but not PO-MSCs-EVs, plays a crucial role in NPs.

RESULTS

Impairment of barrier function and enhancement of EMT in NPs

Barrier function is closely associated with TJs.[34] ZO-1 is the primary constituent of TJs and can be a marker of barrier function.[35] Therefore, we first detected the expression of ZO-1 and EMT-related markers in NPs and inferior turbinate tissues (Patient characteristics detail in Table 1). ZO-1 was expressed at low levels in NPs compared with that in control tissues (Figures 1A and 1B). Moreover, the epithelial marker E-cadherin was markedly downregulated, whereas TGF-β1, N-cadherin, and Vimentin were upregulated in NPs compared with controls (Figures 1C and 1D). Immunohistochemical analysis was consistent with these findings (Figures 1E and 1F), and correlation analysis between ZO-1 and the EMT phenotype indicated a significant correlation. Indeed, ZO-1 immunoreactivity was significantly positively associated with E-cadherin expression and negatively correlated with N-cadherin and Vimentin expression in NPs tissues (Figures 1G–1I). Taken together, these results demonstrated the aberrant EMT and barrier functions in NPs.

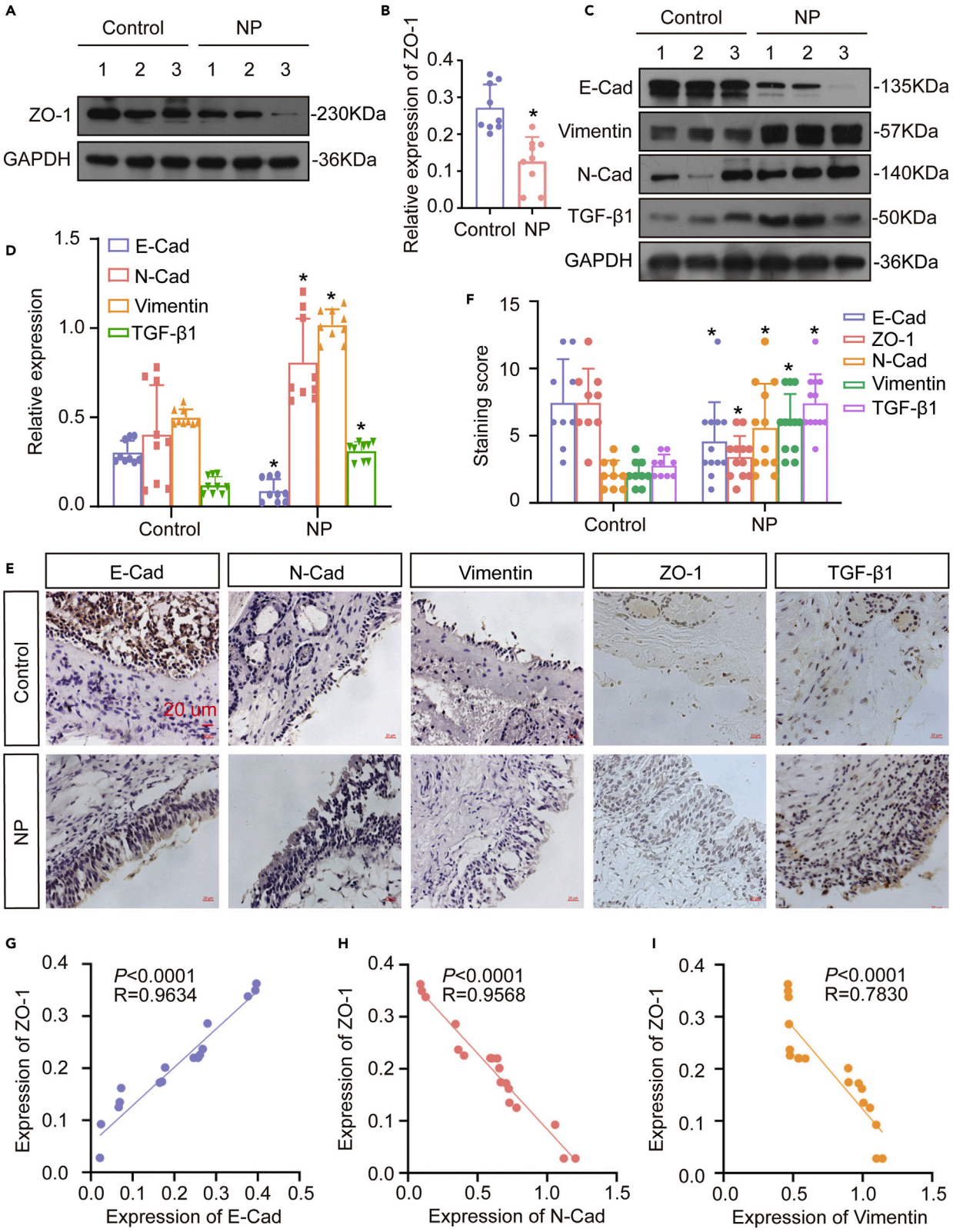

Figure 1. Expression of ZO-1, TGF-β1, and EMT-related phenotypes in NPs tissues

(A and C) Protein expression of (A) ZO-1, (C) TGF-β1, and EMT markers in control and NPs tissues, as detected via western blot. GAPDH was used as a loading control.

Figure 1. *Continued*

(B and D) The intensities of protein bands were quantified using densitometry and normalized to GAPDH expression.

(E) Expression of ZO-1, TGF-β1, and EMT markers in tissues, as measured via immunohistochemical analysis. Scale bar: 20 μm.

(F) Comparison of immunohistochemical staining scores between control and NPs tissues.

(G–I) Correlation analysis of ZO-1, N-cadherin, Vimentin, and E-cadherin. All data represent the mean ± SEM of three independent experiments. *p< 0.05 compared with the control. NPs, nasal polyps; Control, control tissues; IHC, immunohistochemistry; EMT, epithelial-to-mesenchymal transition; ZO-1, zona occludens-1; TGF-β1, transforming growth factor β1; E-Cad, E-cadherin; N-Cad, N-cadherin.

TGF-β1 treatment enhanced EMT and barrier disruption of pHNECs *in vitro*

Next, TGF-β1 was uesd to induce EMT[15,36] to explore the underlying molecular mechanisms of the local microenvironment in pHNECs. Stimulation of TGF-β1 downregulated ZO-1 and E-cadherin and upregulated Vimentin in pHNECs, which indicated that pHNECs underwent EMT (Figures 2A and 2B). Moreover, wound-healing assays showed that the migratory abilities of pHNECs were markedly enhanced after TGF-β1 stimulation (Figures 2C and 2D). ZO-1 (green) and Occludin (red) abundances staining were determined by immunofluorescence (IF) to assess barrier function. The results showed that TGF-β1 promoted disruption of epithelial integrity (Figures 2E and 2F). Destruction of the epithelial barrier is mainly manifested as an increase in epithelial cell permeability. Therefore, dextran labeling was used to assess the permeability changes of the pHNECs treated with TGF-β1. As shown in Figure 2G, the permeability of pHNECs was increased after TGF-β1 stimulation, which was consistent with the increased permeability of NPs. Thus, TGF-β1 induced EMT and facilitated the loss of epithelial integrity.

PO-MSCs promoted the EMT and epithelial barrier destruction in pHNECs

NPs tissues are a source of MSCs, which maintain stemness, differentiation, and clonogenicity capabilities *in vitro*.[10] In this study, PO-MSCs showed a typical spindle-shaped morphology, and differentiation potential into mesodermal lineages such as osteocytes and adipocytes (Figure 3A). The flow cytometry immunophenotyping analysis revealed positive expression of the mesenchymal surface markers CD73, CD90 and CD105 with absence of the hematopoietic surface marker CD34, CD45 and HLA-DR (Figure 3B). Then, labeling of PO-MSCs with CD105, CD73and CD90 in frozen NPs tissue sections revealed PO-MSCs mainly located in the epithelial layer (Figure 3C). These observations supported the role of PO-MSCs in targeting the damaged NPs epithelium, which may directly regulate epithelial barrier function.

Next, pHNECs were co-cultured with PO-MSCs to investigate the potential roles of PO-MSCs on EMT and epithelial barrier function. Meanwhile, TGF-β1 was utilized as a positive control to assess the change of EMT. Similar results were obtained with TGF-β1 treatment. Western blot revealed that ZO-1, Occludin, Claudin-1 and E-cadherin were substantially downregulated, whereas N-cadherin and Vimentin were upregulated after co-culture with PO-MSCs (Figure 3D). Besides, RT-qPCR analysis confirmed these results at mRNA level (Figure 3E). Wound-healing assays showed that PO-MSCs promoted migration ability of pHNECs as well as TGF-β1(Figure 3F). Subsequently, ZO-1 (green) and Occludin (red) immunofluorescence staining demonstrated that, like TGF-β1, PO-MSCs further strengthened the destruction of the epithelial barrier (Figures 3G and 3H). Permeability assays also showed that, as expected, PO-MSCs promoted the permeability ability of pHNECs (Figure 3I). Overall, these findings indicated that PO-MSCs facilitated the EMT and epithelial barrier destruction, which may contribute to NPs formation and progression.

Conditioned medium from PO-MSCs (CM), but not extracellular vesicles derived from PO-MSCs (PO-MSCs-EVs), was crucial for PO-MSCs functions

MSCs are recruited to pathological microenvironments and secrete EVs with the same effects as MSCs.[21,37] To further confirm whether PO-MSCs regulated the EMT and epithelial barrier function by secreting EVs, we isolated EVs from PO-MSCs (PO-MSCs-EVs). Western blot analysis demonstrated that specific EVs markers, such as ALIX, TSG101, CD9, CD63, and flotillin-1 were highly enriched, whereas neither actinin-4 and albumin were not expressed in PO-MSCs-EVs (Figure 4A). TEM analysis demonstrated that the EVs had a typical lipid bilayer morphology (Figure 4B). Furthermore, PKH-67 labeling indicated that PO-MSCs-EVs were taken up by pHNECs (Figure 4C). At the same time, we treated PO-MSCs with the EVs biosynthesis inhibitor GW4869[38] and harvested CM.

Next, PO-MSCs, PO-MSCs-EVs and CM were co-cultured with pHNECs, then changes in EMT and barrier function were evaluated. TGF-β1 was a positive control to assess the change of EMT. Surprisingly, western blot showed that CM, like PO-MSCs, promoted EMT and impaired epithelial barrier function, as evidenced

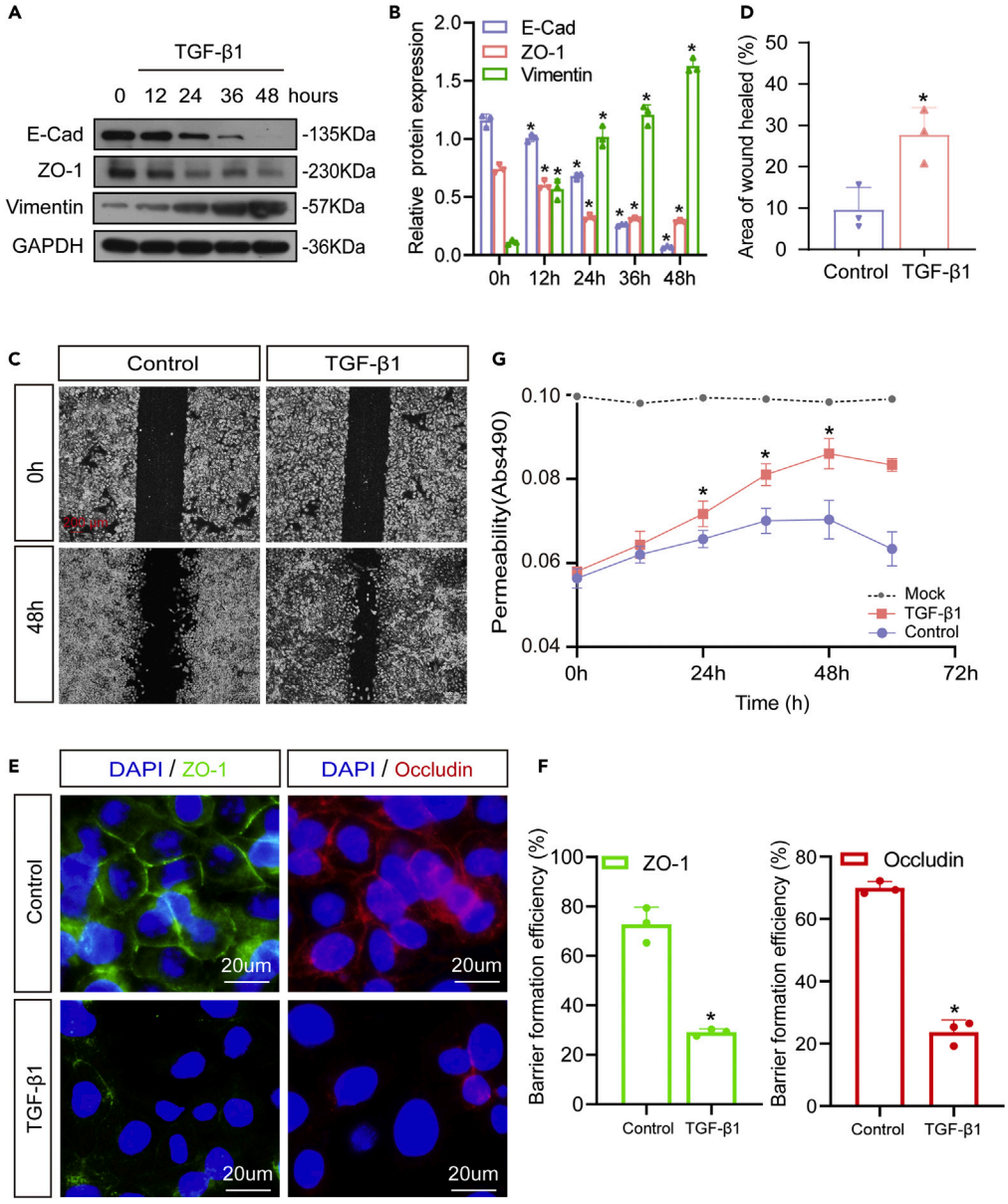

Figure 2. TGF-β1 induced EMT and barrier disruption in pHNECs

(A) Protein expression of ZO-1, E-cadherin and Vimentin after stimulation, as detected via western blot at different times.

(B) The intensities of protein bands were quantified using densitometry and normalized to GAPDH.

(C) Wound-healing assays were used to determine the effects of TGF-β1 on the migration of pHNECs. Scale bar: 200 μm.

(D) Analysis of the relative area of wound healed rate of cells in wound-healing assays.

(E) Representative immunofluorescence photomicrographs of ZO-1 and Occludin showing changes in cellular tight junctions after TGF-β1 stimulation. Scale bar: 20 μm.

(F) Quantification of total extent of barrier formation efficiency in each treatment group. Five visual fields were randomly selected in each microscopic field and counted the number of cells forming tight intercellular adhesions. Each point represents the mean of five visual fields.

(G) Permeability of pHNECs treated with TGF-β1, as measured via permeability assays. All data represent the mean ± SEM of three independent experiments. *p< 0.05 compared with the control or 0 h group. E-Cad, E-cadherin; ZO-1, zona occludens-1; TGF-β1, transforming growth factor β1; Mock, mock treated.

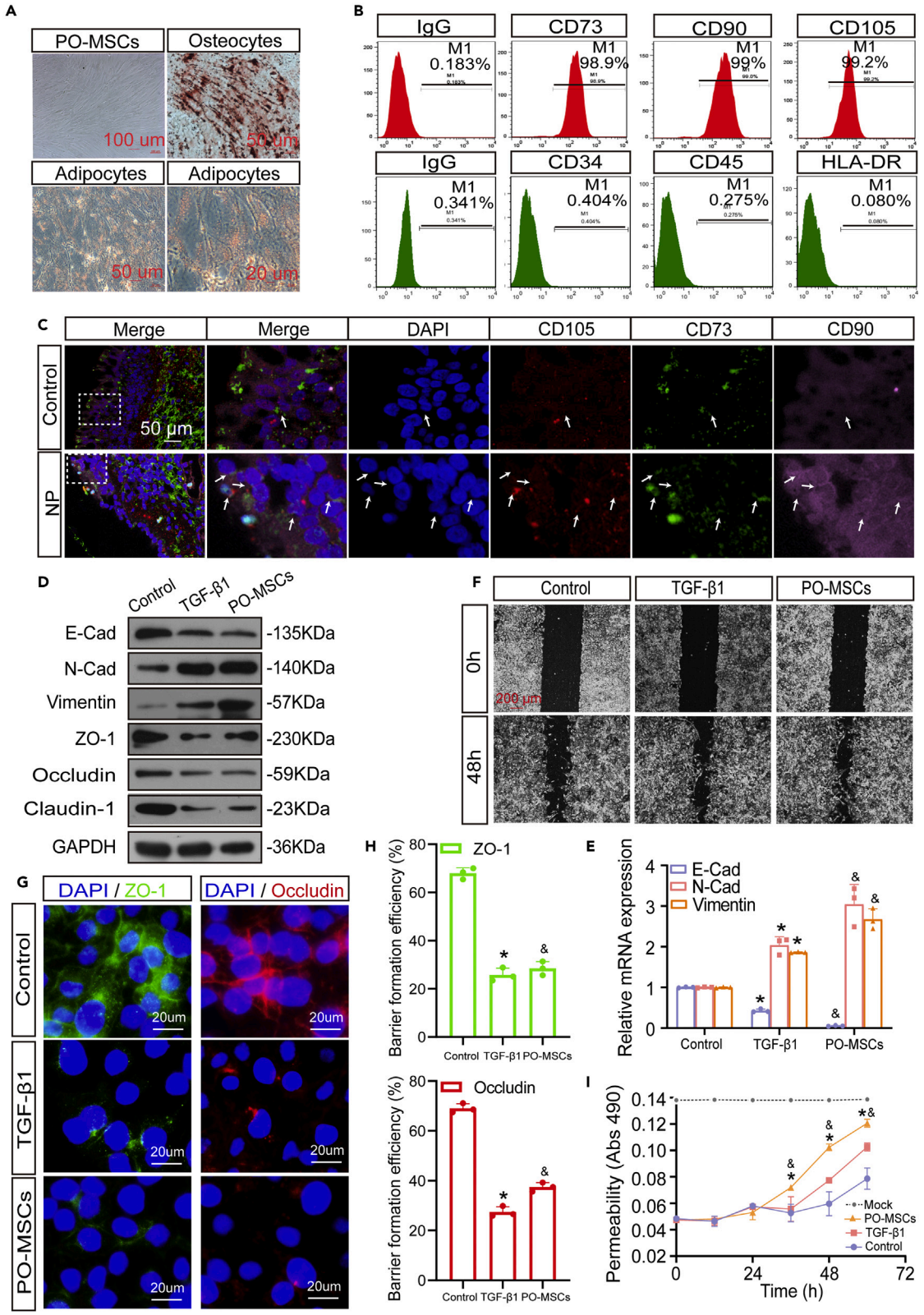
A
PO-MSCs
Osteocytes
100 um
50 um
Adipocytes
Adipocytes
50 um
20 um
B
IgG
M1
0.183%
CD73
M1
98.9%
CD90
M1
99%
CD105
M1
99.2%
IgG
M1
0.341%
CD34
M1
0.404%
CD45
M1
0.275%
HLA-DR
M1
0.080%
C
Merge
Merge
DAPI
CD105
CD73
CD90
Control
NP
50 μm
D
Control
TGF-β1
PO-MSCs
E-Cad
-135KDa
N-Cad
-140KDa
Vimentin
-57KDa
ZO-1
-230KDa
Occludin
-59KDa
Claudin-1
-23KDa
GAPDH
-36KDa
F
Control
TGF-β1
PO-MSCs
0h
48h
200 μm
G
DAPI / ZO-1
DAPI / Occludin
Control
TGF-β1
PO-MSCs
20um
H
ZO-1
Barrier formation efficiency (%)
Control TGF-β1 PO-MSCs
Occludin
Barrier formation efficiency (%)
Control TGF-β1 PO-MSCs
E
E-Cad
N-Cad
Vimentin
Relative mRNA expression
Control
TGF-β1
PO-MSCs
I
Permeability (Abs 490)
Time (h)
Mock
PO-MSCs
TGF-β1
Control

Figure 3. PO-MSCs promoted EMT and epithelial barrier destruction in pHNECs

(A) Microscopy reveals monolayer morphology of PO-MSCs. Scale bar:100 μm. Adipogenic and osteogenic differentiation potential of PO-MSCs. Scale bar:20 μm and 50 μm.

(B) Flow cytometry analyses showed the both positive and negative surface markers of PO-MSCs.

(C) Immunofluorescence staining of PO-MSCs markers (CD105, CD73, CD90) demonstrated the localization of PO-MSCs in the epithelial layer of NPs tissues. Scale bar:50 μm.

(D) Analysis of protein expression of ZO-1, Occludin, Claudin-1 and EMT markers in pHNECs treated with TGF-β1 or co-cultured with PO-MSCs, as examined using western blot.

(E) RT-qPCR showed the mRNA expression levels of EMT markers in pHNECs treated with TGF-β1 or co-cultured with PO-MSCs.

(F) Wound-healing assays were used to detect the relative migration rates of pHNECs. Scale bar: 200 μm.

(G) Representative immunofluorescence photomicrographs of ZO-1 and Occludin showing changes in cellular tight junctions of pHNECs under different stimulation. Scale bar: 20 μm.

(H) Quantification of total extent of barrier formation efficiency in each treatment group. Five visual fields were randomly selected in each microscopic field and counted the number of cells forming tight intercellular adhesions. Each point represents the mean of five visual fields.

(I) Permeability assays were used to measure the paracellular permeability of pHNECs. All data represent the mean ± SEM of three independent experiments. * $^{\&}p< 0.05$ compared with the control group. RT-qPCR, reverse transcription quantitative polymerase chain reaction (qPCR). ZO-1, zona occludens-1; TGF-β1, transforming growth factor β1; E-Cad, E-cadherin; N-Cad, N-cadherin. Mock, mock treated.

by reduction in ZO-1, Occludin, Claudin-1 and E-cadherin and increase in Vimentin and N-cadherin, as compared to PO-MSCs-EVs (Figure 4D). Correspondingly, RT-qPCR analysis indicated the same results at the mRNA level (Figure 4E). In addition, wound-healing assays also suggested that CM significantly promoted pHNECs migration ability as same as PO-MSCs (Figure 4F). Consistent with above findings, permeability assays and immunofluorescence staining showed that both PO-MSCs and CM significantly enhanced permeability and epithelial barrier destruction compared with PO-MSCs-EVs, and CM had the strongest effects (Figures 4G, 4H and 4I). Collectively, these findings indicated that CM, but not PO-MSCs-EVs, significantly enhanced EMT and epithelial barrier destruction in pHNECs.

PO-MSCs derived IGFBP2 promoted EMT and epithelial barrier destruction in pHNECs

MSCs exert their functions through the secretome, including soluble proteins, nucleic acids, and lipids, which show similar effects to those MSCs.[39,40] Therefore, we next investigated whether PO-MSCs promoted EMT and epithelial barrier destruction in pHNECs by secreted proteins, including IGFBP2, matrix metalloproteinase 9 (MMP9), monocyte chemotactic protein-1 (MCP-1), vascular endothelial growth factor A (VEGFA) and interleukin-1β (IL-1β), all of which are associated with pathogenic biological behaviors.[26,41,42] Remarkably, compared with mock control and PO-MSCs-EVs, only IGFBP2 was significantly enriched in PO-MSCs-CM (Figure 5A). Moreover, we also examined the levels of IGFBP2, TGF-β1, MMP9, MCP-1, VEGFA and IL-1β in CM from PO-MSCs and inferior turbinate tissues derived MSCs (C-MSCs). Western blot found that only IGFBP2 was only significant differentially enriched in PO-MSCs-CM compared with C-MSCs-CM, whereas TGF-β1 and MMP-9 enriched both in two cells, but no obvious alteration was observed between them (Figure 5B). Next, we evaluated the roles of IGFBP2 in pHNECs. As shown in Figures 5C and 5D, stimulation of IGFBP2 markedly promoted EMT and epithelial barrier destruction, which was consistent with the treatment by PO-MSCs. We also found that silencing IGFBP2 in PO-MSCs was associated with inhibition of EMT and epithelial barrier destruction of pHNECs by transfecting with siRNA against IGFBP2. Further analyses showed that IGFBP2 was mainly expressed by CD73-positive and CD105-positive PO-MSCs in NPs tissues. Notably, co-localization of IGFBP2 and PO-MSCs on the epithelium and lamina propria was clearly observed in NPs (Figure 5E). Subsequently, we explored the correlations between PO-MSCs, ZO-1 and deposition of IGFBP2, and the results showed that ZO-1 downregulation was related to PO-MSCs infiltration and IGFBP2 enrichment, with an inverse association (Figure 5F). As expected, correlative analysis showed that the number of PO-MSCs is inversely proportional to the expression of ZO-1 and positively correlated with IGFBP2. The fluorescence intensity analysis showed a negative correlation between ZO-1 and IGFBP2 (Figures 5G–5I). TGF-β1, as a positive control in this study, is a cytokine with pleiotropic functions including regulation of extracellular matrix remodeling. In humans, TGF-β1 has been found to be the most abundant isoform and is widely expressed by most cells.[43] We found that TGF-β1 was enriched both in PO-MSCs-CM and C-MSCs-CM, but no obvious difference was observed between them. To verify the relation among TGF-β1 with PO-MSCs and ZO-1 via Immunofluorescence staining. The results showed that ZO-1 reduction was associated with both CD73-positive PO-MSCs infiltration and TGF-β1 enrichment in NPs (Figure 5J). To further clarify the major facilitator in EMT and epithelial barrier destruction of PO-MSCs, immunofluorescence staining and ELISA were performed to probe the cellular origin of TGF-β1 in the NPs microenvironment. The results showed that TGF-β1 was derived from fibroblasts, neutrophils, eosinophils and PO-MSCs, especially dominated

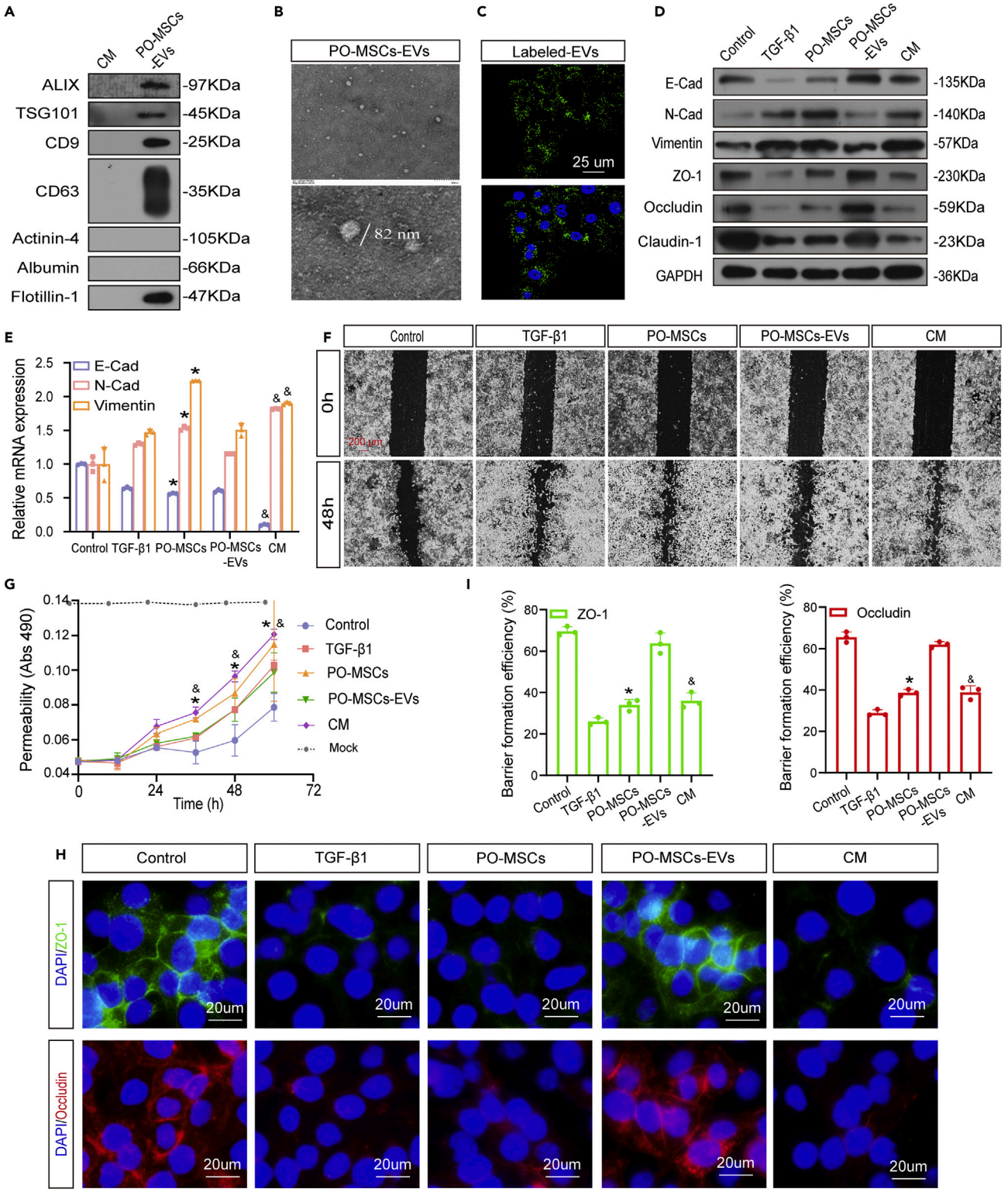

Figure 4. CM enhanced EMT and epithelial barrier destruction in pHNECs

(A) Western blot detected the EVs markers.

(B) Transmission electron microscopy of PO-MSCs-EVs. Scale bar: 200 nm.

(C) Confocal microscopy analysis of the uptake of PKH67-labeled (green fluorescence) PO-MSCs-EVs by pHNECs. Scale bar: 25 μm.

Figure 4. *Continued*

(D) Western blot detected the epithelial barrier and EMT-related markers.

(E) RT-qPCR detected the mRNA expression levels of EMT-related markers.

(F)Wound-healing assays were used to detect the migration ability of pHNECs. Scale bar: 200 nm.

(G) Permeability assays were used to measure the paracellular permeability of pHNECs.

(H) Representative immunofluorescence photomicrographs of ZO-1 and Occludin showing changes in cellular tight junctions of pHNECs under different stimulation. Scale bar: 20 μm.

(I) Quantification of total extent of barrier formation efficiency in each treatment group. Five visual fields were randomly selected in each microscopic field and counted the number of cells forming tight intercellular adhesions. Each point represents the mean of five visual fields. All data represent the mean ± SEM of three independent experiments. *p< 0.05 compared with the control group. $^{\&}$p< 0.05 compared with the control and PO-MSCs-EVs co-culture group. RT-qPCR, reverse transcription qPCR. ZO-1, zona occludens-1; TGF-β1, transforming growth factor β1; E-Cad, E-cadherin; N-Cad, N-cadherin. Mock, mock treated.

by fibroblasts rather than PO-MSCs, which is consistent with previous studies[44] (Figures S1A–S1E). Meanwhile, ELISA was performed to detect the expression of IGFBP2 in pHNECs and those above cells, the results suggested IGFBP2 was significantly enriched in PO-MSCs (Figure S1F). Finally, to determine whether the role of IGFBP2 is related to TGF-β1, we added si-TGF-β1 to block the effects of it in PO-MSCs before co-culture with PHNECs. Our results showed that PO-MSCs still promoted EMT and epithelial damage, even in the presence of TGF-β1 knockdown, which indicating that IGFBP2 does not rely upon TGF-β1 for its role (Figure 5K). Taken together, these results suggested that IGFBP2 was essential for EMT and epithelial damage caused by PO-MSCs in NPs microenvironment.

Secreted IGFBP2 activated the FAK pathway to mediate dysregulation of EMT and epithelial barrier function in NPs

To further investigate the mechanism by which IGFBP2 induces EMT and barrier destruction, we focused on the FAK pathways. We first evaluated the activation state of FAK in IGFBP2-treated pHNECs. As shown in Figure 6A, in comparison with total FAK, phosphorylated FAK (*p*-FAK) activation was observed after IGFBP2 stimulation or incubation with PO-MSCs, and downstream phosphorylated MEK1/2 (*p*-MEK1/2) was also enhanced. In the light of the crucial function of *p*-FAK in EMT, which was regulated by IGFBP2, we performed rescue experiments using PF573228 (a FAK-specific inhibitor[45,46]) to investigate the relative contributions of FAK pathways to IGFBP2-mediated EMT and barrier destruction. pHNECs derived from NPs tissues (PO-pHNECs) were stimulated with different concentrations of PF573228 (0, 2.5, 5 and 10 μmol) for 6 and 12 h, and then harvested for future experiments. We first evaluated the effects of concentration and exposure time of various treatments of the PF573228. Western blot showed that the active suppressive effect of the FAK inhibitor was dose- and time-dependent (Figures S2A and S2B). Treatment of PO-pHNECs with PF573228 resulted in upregulation of ZO-1, Occludin, Claudin-1 and E-cadherin, but downregulation of IGFBP2, vimentin, and N-cadherin. Meanwhile, we also found that suppression of FAK activity with PF573228 significantly inhibited EMT and barrier destruction mediated by IGFBP2. Reciprocally, suppression of FAK activity rescued EMT process and barrier destruction in IGFBP2-silenced pHNECs (Figure 6B). Wound-healing assays also showed that pHNECs migration was inhibited by PF573228compared with IGFBP2 alone. However, the combination of the two reagents rescued the inhibitory effects (Figures 6C and 6D). Finally, as further validation of these results, immunofluorescence and permeability assays showed that PF573228 alone increased ZO-1 and Occludin expression and decreased permeability. By contrast, the combination of PF573228 and IGFBP2 partially neutralized this suppressive effect (Figures 6E–6G). Taken together, these findings illustrated that the FAK signaling pathway was a crucial mechanism by which PO-MSCs-secreted IGFBP2 mediated EMT and barrier destruction in NPs microenvironment.

FAK is essential for IGFBP2 to promote EMT and barrier destruction of nasal mucosa *in vivo*

To this end, we performed *in vivo* experiments to further certify our findings *in vitro* experiments. The detailed description of the operation method is shown in Figure 7A. At the scheduled time, mice were killed after anesthesia and collected the sinonasal specimens. As shown in Figure 7B, exogenous IGFBP2 stimulation promoted the destruction of epithelial junctions, thickened basement membrane, and eosinophil infiltration in the nasal mucosa of mice, which is in line with the TGF-β1 positive control do. As expected, the high concentration of IGFBP2 (20 μg/kg) showed more dramatic in epithelial injury and treatment with the FAK inhibitor PF573228 can reverse the effects of IGFBP2 in mice model. We next examined the expression of IGFBP2 and EMT markers by immunofluorescence assay. The results displayed a co-localization among IGFBP2, E-cadherin and Vimentin in nasal epithelial layers of mice under

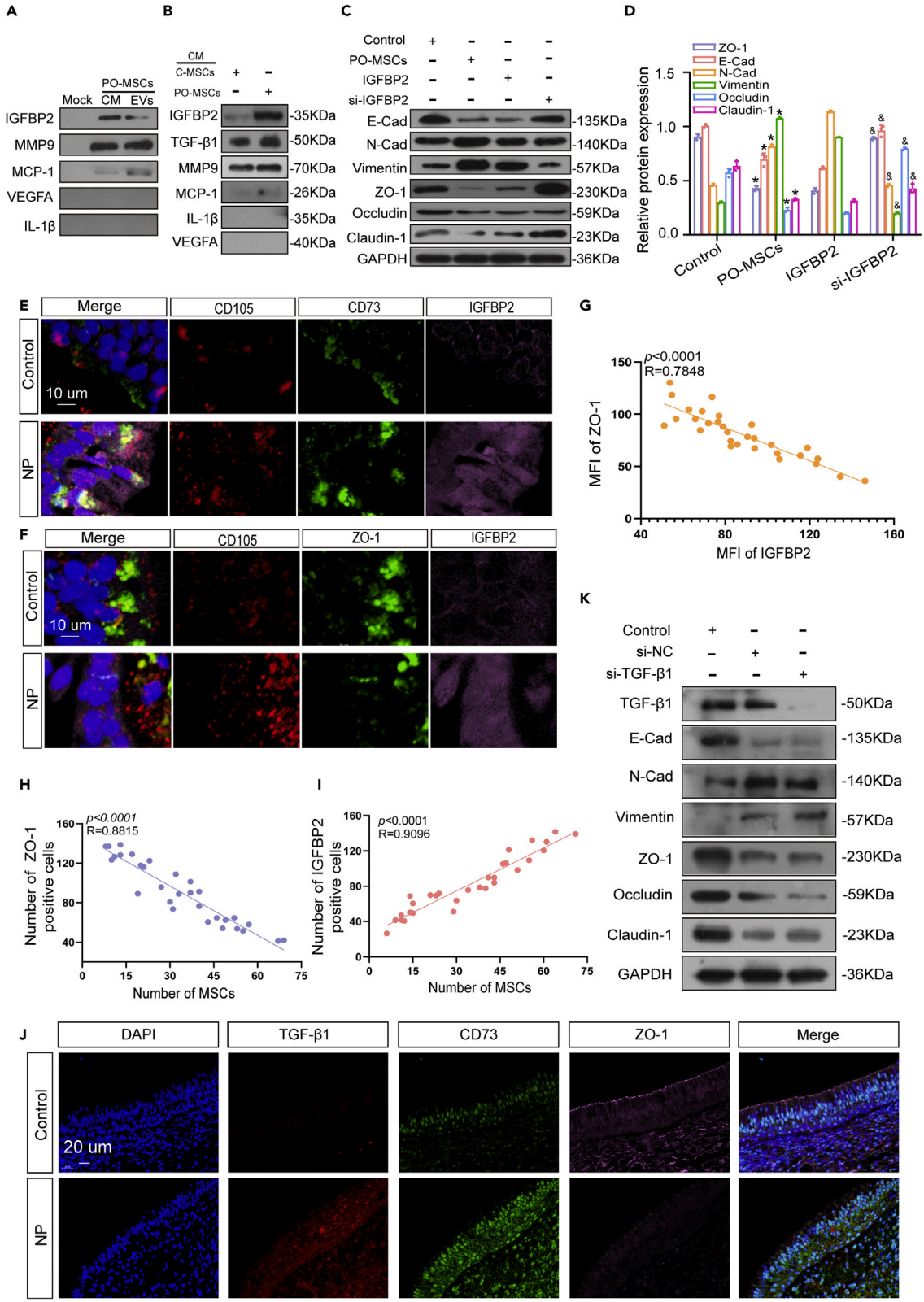
A
Mock
PO-MSCs
CM
EVs
IGFBP2
MMP9
MCP-1
VEGFA
IL-1β
B
CM
C-MSCs
PO-MSCs
IGFBP2
TGF-β1
MMP9
MCP-1
IL-1β
VEGFA
-35KDa
-50KDa
-70KDa
-26KDa
-35KDa
-40KDa
C
Control
PO-MSCs
IGFBP2
si-IGFBP2
E-Cad
N-Cad
Vimentin
ZO-1
Occludin
Claudin-1
GAPDH
-135KDa
-140KDa
-57KDa
-230KDa
-59KDa
-23KDa
-36KDa
D
ZO-1
E-Cad
N-Cad
Vimentin
Occludin
Claudin-1
Relative protein expression
Control
PO-MSCs
IGFBP2
si-IGFBP2
E
Merge
CD105
CD73
IGFBP2
Control
NP
10 um
F
Merge
CD105
ZO-1
IGFBP2
Control
NP
10 um
G
p<0.0001
R=0.7848
MFI of ZO-1
MFI of IGFBP2
H
p<0.0001
R=0.8815
Number of ZO-1 positive cells
Number of MSCs
I
p<0.0001
R=0.9096
Number of IGFBP2 positive cells
Number of MSCs
K
Control
si-NC
si-TGF-β1
TGF-β1
E-Cad
N-Cad
Vimentin
ZO-1
Occludin
Claudin-1
GAPDH
-50KDa
-135KDa
-140KDa
-57KDa
-230KDa
-59KDa
-23KDa
-36KDa
J
DAPI
TGF-β1
CD73
ZO-1
Merge
Control
NP
20 um

Figure 5. PO-MSCs derived IGFBP2 promoted the EMT process and epithelial barrier disruption in pHNECs

(A and B) Western blot detected the expression levels of different soluble proteins.

(C) Western blot detected the epithelial barrier and EMT-related markers in pHNECs.

(D) The intensities of protein bands were quantified using densitometry and normalized to GAPDH expression.

(E) Immunofluorescence staining of CD105, CD73 and IGFBP2 in tissues. Scale bar: 10 μm.

(F) Immunofluorescence staining of CD105, ZO-1 and IGFBP2 in tissues. Scale bar: 10 μm.

(G) Pearson correlations between ZO-1 and IGFBP2.

(H and I) Pearson correlations among ZO-1, IGFBP2 and PO-MSCs numbers.

(J) Immunofluorescence staining of TGF-β1, CD73 and ZO-1 in tissues. Scale bar: 20 μm.

(K) Western blot detected the epithelial barrier and EMT-related markers in pHNECs. All data represent the mean ± SEM of three independent experiments. *p< 0.05 compared with the control group. &p< 0.05 compared with the IGFBP2 treated group. ZO-1, zona occludens-1; E-Cad, E-cadherin; N-Cad, N-cadherin. MMP9, matrix metalloproteinase 9; MCP-1, monocyte chemotactic protein-1; VEGFA, vascular endothelial growth factor A; IL-1β, interleukin-1β.

the IGFBP2 stimulation, but these changes blocked in the presence of PF573228 (Figures 7C and 7D). Meanwhile, immunofluorescence assay also showed that exogenous IGFBP2 stimulation resulted in ZO-1 downregulation, whereas the addition of PF573228 reversed IGFBP2-induced ZO-1 reduction and barrier disruption in mice. (Figures 7E and 7F). To further confirm that we performed histochemical assay again. The results were consistent with above data (Figures S3A and S3B). In sum, our experimental data from *in vivo* assay illustrated that IGFBP2 mediated EMT and epithelial barrier dysfunction through the FAK signaling pathway, which was concordant with the *in vitro* findings.

DISCUSSION

CRSwNP is a common chronic inflammatory disease of the respiratory tract, affecting approximately 0.5–4% of the total population,[1] causing considerable reductions in patient quality of life, and increasing the economic burden on society. EMT and mucosal epithelial barrier disruption are commonly observed in NPs and are crucial for elucidating the mechanisms that underlie the development of NPs.[2,5,15] The barrier function of the nasal mucosa is orchestrated by epithelial cell-cell junctions, including apical TJs and underlying adherens junctions.[47] Particularly critical for maintaining epithelial integrity, ZO-1, Occludin and Claudin-1 are important component of TJs.[35] During EMT, intercellular adhesions and junctions are weakened, nasal mucosa is damaged and basement membrane thickens, ultimately leading to NPs formation.[48] In this study, we confirmed the downregulation of ZO-1 and aberrant epithelial barrier function in tissues and pHNECs in NPs microenvironment. Moreover, EMT was involved in NPs, consistent with previous findings.[4,6] However, certain factors still require consideration. Although emerging evidence highlights the important role of the microenvironment containing various cell types and bioactive molecules in the pathogenesis of NPs,[8,49] the specific underlying molecular mechanisms have not yet been fully elucidated, particularly in regarding the role of PO-MSCs in the pathogenesis of NPs.

MSCs can be isolated from various tissues and effectively cultured *in vitro*. PO- MSCs, a type of MSCs derived from NPs tissues, have the basic characteristics of MSCs, but share different gene expression profiles compared with BM-MSCs.[8] In addition, Chiarella et al. showed that although PO-MSCs exhibit the same typical antigen expression as MSCs from non-NPs mucosa tissues, they are deficient in adipose differentiation.[50] These results suggest that PO-MSCs may play roles different from other MSCs in the local microenvironment of the nasal cavity, which may be implicated in the development of NPs. Thus, in the current study, we assessed the impact of PO-MSCs on modulation of the NPs microenvironment. First, we isolated PO-MSCs from fresh NPs tissues. After characterization of the PO-MSCs phenotype and differentiation, the cells were co-cultured with pHNECs, and destruction of the epithelial barrier was observed. We found that ZO-1, Occludin, Claudin-1 and E-cadherin were downregulated, whereas N-cadherin and Vimentin were upregulated in pHNECs after co-treatment with PO-MSCs, indicating that PO-MSCs act similarly to TGF-β1. Moreover, PO-MSCs promoted migration and permeability of pHNECs. These findings revealed that PO-MSCs damaged the NPs epithelium, directly driving epithelial barrier dysfunction and EMT.

MSCs affect the pathological process by secreting EVs and secretome.[19–21] Intriguingly, MSCs-EVs play important roles in inflammatory diseases and have promising roles in various treatments.[37,51] However, in this study, we found that CM obtained from PO-MSCs treated with GW4869, but not PO-MSCs-EVs, played crucial roles in destroying the epithelial barrier of pHNECs. Accordingly, we hypothesize that the soluble factors released by PO-MSCs may modulate the inflammatory microenvironment of NPs. Among the identified PO-MSCs derived pathogenic proteins, we focused on IGFBP2, which regulates EMT.[52]

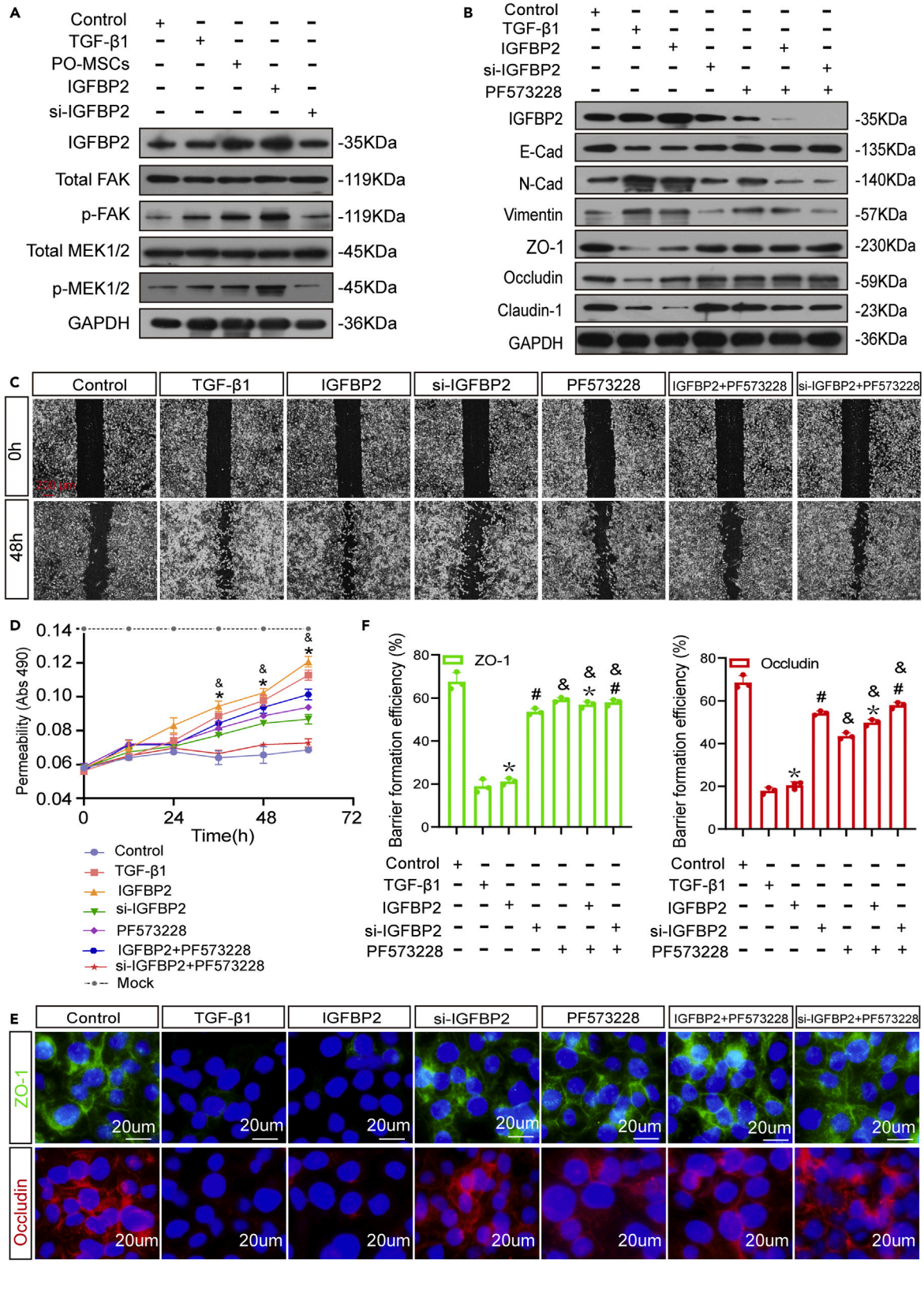
A
Control
TGF-β1
PO-MSCs
IGFBP2
si-IGFBP2
IGFBP2
-35KDa
Total FAK
-119KDa
p-FAK
-119KDa
Total MEK1/2
-45KDa
p-MEK1/2
-45KDa
GAPDH
-36KDa
B
Control
TGF-β1
IGFBP2
si-IGFBP2
PF573228
IGFBP2
-35KDa
E-Cad
-135KDa
N-Cad
-140KDa
Vimentin
-57KDa
ZO-1
-230KDa
Occludin
-59KDa
Claudin-1
-23KDa
GAPDH
-36KDa
C
Control
TGF-β1
IGFBP2
si-IGFBP2
PF573228
IGFBP2+PF573228
si-IGFBP2+PF573228
0h
48h
D
Permeability (Abs 490)
Time(h)
Control
TGF-β1
IGFBP2
si-IGFBP2
PF573228
IGFBP2+PF573228
si-IGFBP2+PF573228
Mock
F
ZO-1
Occludin
Barrier formation efficiency (%)
Control
TGF-β1
IGFBP2
si-IGFBP2
PF573228
E
ZO-1
Occludin
20um

Figure 6. Secreted IGFBP2 activated the FAK pathway to mediate dysregulation of EMT and epithelial barrier function in NPs

(A) Western blot determined the expression of FAK signaling pathway components.

(B) Expression of ZO-1, Occludin, Claudin-1 and EMT markers in pHNECs treated with IGFBP2 or PF573228, as determined using western blot.

(C) Wound-healing assay was used to detect the migration ability of pHNECs treated with IGFBP2 or PF573228.

(D) Permeability of pHNECs treated with IGFBP2 or PF573228, as measured via *in vitro* permeability assays.

(E) Representative immunofluorescence photomicrographs of ZO-1 and Occludin showing changes in cellular tight junctions of pHNECs under different stimulation. Scale bar: 20 μm.

(F) Quantification of total extent of barrier formation efficiency in each treatment group. Five visual fields were randomly selected in each microscopic field and counted the number of cells forming tight intercellular adhesions. Each point represents the mean of five visual fields. All data represent the mean ± SEM of three independent experiments. *$p < 0.05$ compared with the control group. #$p < 0.05$ compared with the IGFBP2-treated group. &$p < 0.05$ compared with the IGFBP2-treated group. *&$p < 0.05$ compared with the IGFBP2-treated and PF573228-treated alone group. # &$p < 0.05$ compared with the si-IGFBP2-treated and PF573228-treated alone group. PF573228: FAK signaling pathway inhibitor; ZO-1, zona occludens-1; TGF-β1, transforming growth factor β1; E-Cad, E-cadherin; N-Cad, N-cadherin. Mock, mock treated.

IGFBP2, as the second most abundant circulating protein, activates inflammatory and immune-related signaling pathways to regulate disease development.[26] In this study, we found that IGFBP2 was significantly enriched in CM and co-localized with PO-MSCs in NPs epithelium. In addition, stimulation of IGFBP2 downregulated ZO-1, Occludin, Claudin-1 and E-cadherin, but upregulated N-cadherin and Vimentin in pHNECs, suggesting IGFBP2 promotes EMT as well as barrier disruption. Simultaneously, our findings showed that there was a correlation between ZO-1 reduction and PO-MSCs infiltration. Collectively, these results suggested that IGFBP2 was essential for the effects of PO-MSCs in promoting EMT and epithelial dysfunction.

Overexpression and activation of FAK is closely associated with cell proliferation, differentiation, migration, and EMT.[30,53,54] In addition, IGFBP2 is significantly associated with FAK phosphorylation.[33] Our findings, together with other studies, suggested that IGFBP2 stimulation could activate FAK and the downstream signaling molecule *p*-MEK1/2.

In summary, our findings indicated that IGFBP2 secreted from PO-MSCs mediated EMT and epithelial barrier dysfunction through the activation of the FAK signaling pathway in the NPs local microenvironment. These findings may improve our current understanding of the roles of PO-MSCs in the NPs microenvironment and ultimately contribute to the prevention and treatment of NPs.

Limitations of the study

However, this current study had several limitations. We constructed an EMT model using TGF-β1, which induced EMT but may partly mirror the pathogenesis of NPs in humans. Importantly, the population heterogeneity of PO-MSCs needs to be further distinguished and explored based on a large population-based sample, which awaits in-depth analysis in follow-up studies. Moreover, to achieve novel PO-MSCs/IGFBP2-targeted therapies, a further trial with bulk specimens and population-based data are warranted to probe the effects of PO-MSCs on NPs physiological processes.

STAR★METHODS

Detailed methods are provided in the online version of this paper and include the following:

- KEY RESOURCES TABLE
- RESOURCE AVAILABILITY
  - Lead contact
  - Materials availability
  - Data and code availability
- EXPERIMENTAL MODEL AND SUBJECT DETAILS
  - Human subjects
  - Experimental animals BALB/c mice
- METHOD DETAILS
  - Cells culture, stimulation and transfection
  - Histology and immunohistochemistry
  - Immunofluorescence and triple fluorescence staining
  - Western blot analysis
  - Reverse transcription quantitative polymerase chain reaction (RT-qPCR)

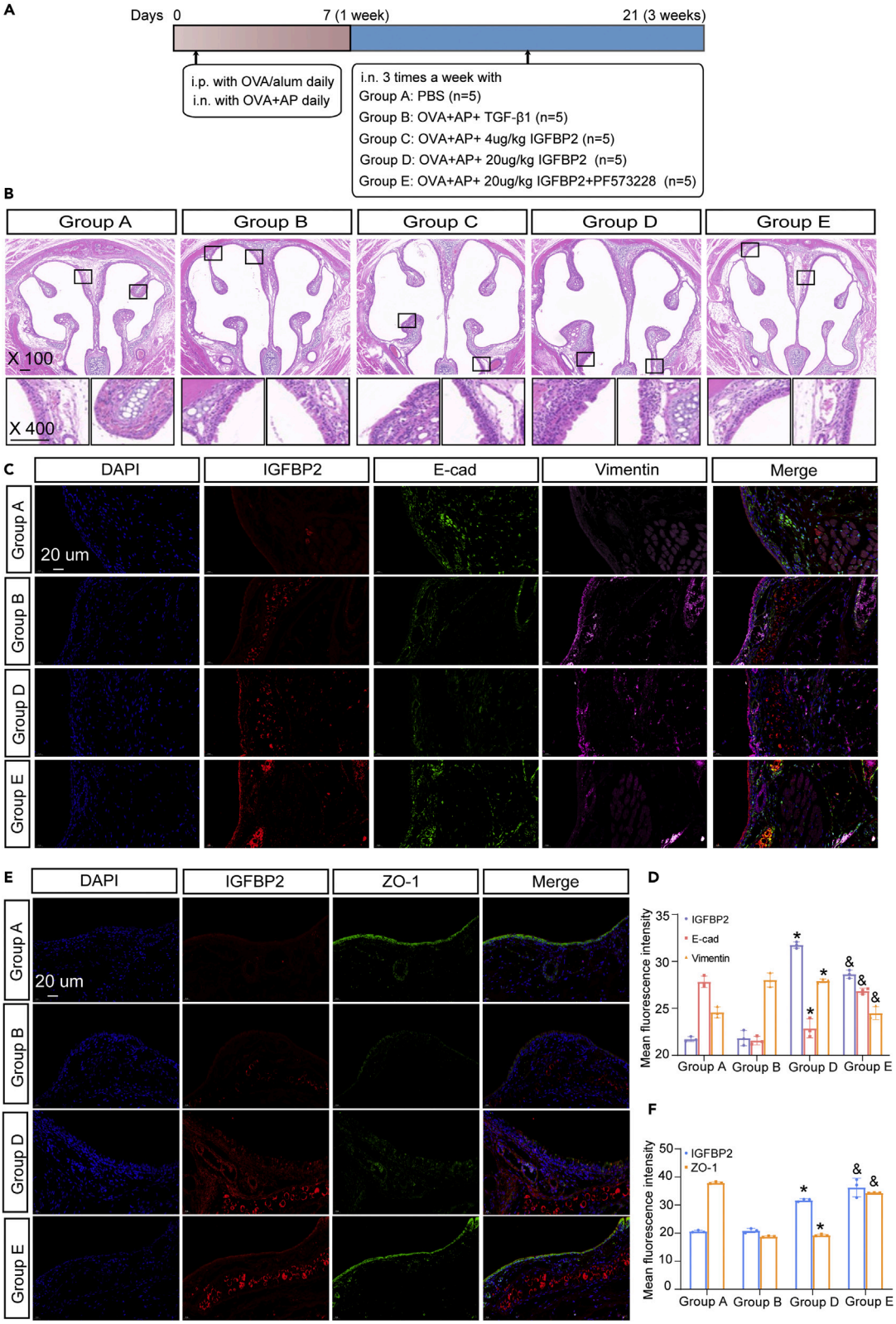
A
Days 0
7 (1 week)
21 (3 weeks)
i.p. with OVA/alum daily
i.n. with OVA+AP daily
i.n. 3 times a week with
Group A: PBS (n=5)
Group B: OVA+AP+ TGF-β1 (n=5)
Group C: OVA+AP+ 4ug/kg IGFBP2 (n=5)
Group D: OVA+AP+ 20ug/kg IGFBP2 (n=5)
Group E: OVA+AP+ 20ug/kg IGFBP2+PF573228 (n=5)
B
Group A
Group B
Group C
Group D
Group E
X 100
X 400
C
DAPI
IGFBP2
E-cad
Vimentin
Merge
Group A
Group B
Group D
Group E
20 um
E
DAPI
IGFBP2
ZO-1
Merge
Group A
Group B
Group D
Group E
20 um
D
Mean fluorescence intensity
IGFBP2
E-cad
Vimentin
Group A
Group B
Group D
Group E
F
Mean fluorescence intensity
IGFBP2
ZO-1
Group A
Group B
Group D
Group E

Figure 7. FAK is essential for IGFBP2 to promote EMT and barrier destruction of nasal mucosa in vivo

(A) Protocol for the mice model. Mice were divided into 5 groups and treated with OVA, AP, and various stimulants. i.p., Intraperitoneal injection; i.n., Intranasal instillation.

(B) H&E staining of the nasal cavity and representative photographs nasal epithelial destruction lesions.

(C) Representative Immunofluorescence staining of IGFBP2, E-cad and Vimentin in mice tissue lesions. Scale bar: 20 μm.

(D) Quantification of fluorescence efficiency in each treatment group.

(E) Representative Immunofluorescence staining of IGFBP2 and ZO-1 in mice tissue lesions. Scale bar: 20 μm.

(F) Quantification of fluorescence efficiency in each treatment group. Five visual fields were randomly selected in each microscopic field and counted the number of cells forming tight intercellular adhesions. Each point represents the mean of five visual fields. All data represent the mean ± SEM of three independent experiments. *p< 0.05 compared with the Group A. #p< 0.05 compared with the Group D. OVA: ovalbumin; AP: *Aspergillus oryzae*; IGFBP2: Insulin-like growth factor binding protein 2; PF573228: FAK signaling pathway inhibitor; ZO-1, zona occludens-1; TGF-β1, transforming growth factor β1; E-Cad, E-cadherin.

SUPPLEMENTAL INFORMATION

Supplemental information can be found online at https://doi.org/10.1016/j.isci.2023.106151.

ACKNOWLEDGMENTS

This research was supported by the Nantong Clinical Research Project (grant no. JC2018103 and MS12021096 to J.C.), Jieping Wu Medical Foundation Clinical Research Project (grant no. 320.6750.18272 to J.C.), and the National Natural Science Foundation of China (NSFC; grant nos. 81970862 to L.C. and 81871278 and 81671616 to Z.F.G.).

AUTHOR CONTRIBUTIONS

B.Y., T.Z., W.Z., Z.F.G., L.C., and J.C. conceived the project and designed the experiments; B.Y., T.Z., W.Z., Y.Y.P., D.Y.H., Y.L., and S.C.Z. performed the experiments and organized the figures; B.Y., T.Z., W.Z., C.Y.Q., and J.Z. analyzed the data; B.Y., T.Z., W.Z., Z.F.G., L.C., and J.C., wrote the manuscript. All authors commented on the manuscript.

DECLARATION OF INTERESTS

The authors declare no competing interests.

Received: June 8, 2022
Revised: November 19, 2022
Accepted: February 2, 2023
Published: February 7, 2023

REFERENCES

1. Fokkens, W.J., Lund, V.J., Hopkins, C., Hellings, P.W., Kern, R., Reitsma, S., Toppila-Salmi, S., Bernal-Sprekelsen, M., Mullol, J., Alobid, I., et al. (2020). European position paper on rhinosinusitis and nasal polyps 2020. Rhinology *58*, 1–464. https://doi.org/10.4193/Rhin20.600.

2. Schleimer, R.P., and Robert, P. (2017). Immunopathogenesis of chronic rhinosinusitis and nasal polyposis. Annu. Rev. Pathol. *12*, 331–357.

3. Bhattacharyya, N., Villeneuve, S., Joish, V.N., Amand, C., Mannent, L., Amin, N., Rowe, P., Maroni, J., Eckert, L., Yang, T., and Khan, A. (2019). Cost burden and resource utilization in patients with chronic rhinosinusitis and nasal polyps. Laryngoscope *129*, 1969–1975. https://doi.org/10.1002/lary.27852.

4. Wang, C., Yan, B., and Zhang, L. (2020). The epithelium-derived inflammatory mediators of chronic rhinosinusitis with nasal polyps. Expert Rev. Clin. Immunol. *16*, 293–310. https://doi.org/10.1080/1744666X.2020.1723417.

5. Jiao, J., Wang, C., and Zhang, L. (2019). Epithelial physical barrier defects in chronic rhinosinusitis. Expert Rev. Clin. Immunol. *15*, 679–688. https://doi.org/10.1080/1744666X.2019.1601556.

6. Jiao, J., Wang, M., Duan, S., Meng, Y., Meng, N., Li, Y., Fan, E., Akdis, C.A., and Zhang, L. (2018). Transforming growth factor-beta1 decreases epithelial tight junction integrity in chronic rhinosinusitis with nasal polyps. J. Allergy Clin. Immunol. *141*, 1160–1163.e9. https://doi.org/10.1016/j.jaci.2017.08.045.

7. Juárez-Navarro, K.J., Padilla-Camberos, E., Díaz, N.F., Miranda-Altamirano, A., and Díaz-Martínez, N.E. (2020). Human mesenchymal

stem cells: the present alternative for high-incidence diseases, even SARS-Cov-2. Stem Cells Int. *2020*, 8892189. https://doi.org/10.1155/2020/8892189.

8. de Oliveira, P.W.B., Pezato, R., Agudelo, J.S.H., Perez-Novo, C.A., Berghe, W.V., Câmara, N.O., de Almeida, D.C., and Gregorio, L.C. (2017). Nasal polyp-derived mesenchymal stromal cells exhibit lack of immune-associated molecules and high levels of stem/progenitor cells markers. Front. Immunol. *8*, 39. https://doi.org/10.3389/fimmu.2017.00039.

9. Salem, H.K., and Thiemermann, C. (2010). Mesenchymal stromal cells: current understanding and clinical status. Stem Cell. *28*, 585–596. https://doi.org/10.1002/stem.269.

10. Klimek, L., Koennecke, M., Mullol, J., Hellings, P.W., Wang, D.Y., Fokkens, W., Gevaert, P., and Wollenberg, B. (2017). A possible role of stem cells in nasal polyposis. Allergy *72*, 1868–1873. https://doi.org/10.1111/all.13221.

11. Yu, X.M., Li, C.W., Chao, S.S., Li, Y.Y., Yan, Y., Zhao, X.N., Yu, F.G., Liu, J., Shen, L., Pan, X.L., et al. (2014). Reduced growth and proliferation dynamics of nasal epithelial stem/progenitor cells in nasal polyps in vitro. Sci. Rep. *4*, 4619. https://doi.org/10.1038/srep04619.

12. Zhao, L., Li, Y.Y., Li, C.W., Chao, S.S., Liu, J., Nam, H.N., Dung, N.T.N., Shi, L., and Wang, D.Y. (2017). Increase of poorly proliferated p63(+)/Ki67(+) basal cells forming multiple layers in the aberrant remodeled epithelium in nasal polyps. Allergy *72*, 975–984. https://doi.org/10.1111/all.13074.

13. Chiarella, E., Lombardo, N., Lobello, N., Aloisio, A., Aragona, T., Pelaia, C., Scicchitano, S., Bond, H.M., and Mesuraca, M. (2020). Nasal polyposis: insights in epithelial-mesenchymal transition and differentiation of polyp mesenchymal stem cells. Int. J. Mol. Sci. *21*, 6878. https://doi.org/10.3390/ijms21186878.

14. Li, J., Zhang, Y., and Zhang, L. (2016). [Features of epithelial-to-mesenchymal transition in nasal polyposis]. Zhonghua er bi yan hou tou jing wai ke za zhi *51*, 174–178. https://doi.org/10.3760/cma.j.issn.1673-0860.2016.03.004.

15. Zhang, T., Zhou, Y., You, B., You, Y., Yan, Y., Zhang, J., Pei, Y., Zhang, W., and Chen, J. (2021). miR-30a-5p inhibits epithelial-to-mesenchymal transition by targeting CDK6 in nasal polyps. Am. J. Rhinol. Allergy *35*, 152–163. https://doi.org/10.1177/1945892420939814.

16. Zhang, W., Zhang, T., Yan, Y., Zhang, J., Zhou, Y., Pei, Y., Yao, L., You, B., and Chen, J. (2020). Exosomal miR-22-3p derived from chronic rhinosinusitis with nasal polyps regulates vascular permeability by targeting VE-cadherin. BioMed Res. Int. *2020*, 1237678. https://doi.org/10.1155/2020/1237678.

17. Zhang, W., Zhang, J., Cheng, L., Ni, H., You, B., Shan, Y., Bao, L., Wu, D., Zhang, T., Yue, H., and Chen, J. (2018). A disintegrin and metalloprotease 10-containing exosomes derived from nasal polyps promote angiogenesis and vascular permeability. Mol. Med. Rep. *17*, 5921–5927. https://doi.org/10.3892/mmr.2018.8634.

18. Timaner, M., Tsai, K.K., and Shaked, Y. (2020). The multifaceted role of mesenchymal stem cells in cancer. Semin. Cancer Biol. *60*, 225–237. https://doi.org/10.1016/j.semcancer.2019.06.003.

19. Volarevic, V., Gazdic, M., Simovic Markovic, B., Jovicic, N., Djonov, V., and Arsenijevic, N. (2017). Mesenchymal stem cell-derived factors: Immuno-modulatory effects and therapeutic potential. Biofactors *43*, 633–644. https://doi.org/10.1002/biof.1374.

20. Zhu, W., Huang, L., Li, Y., Qian, H., Shan, X., Yan, Y., Mao, F., Wu, X., and Xu, W.R. (2011). Mesenchymal stem cell-secreted soluble signaling molecules potentiate tumor growth. Cell Cycle *10*, 3198–3207. https://doi.org/10.4161/cc.10.18.17638.

21. Keshtkar, S., Azarpira, N., and Ghahremani, M.H. (2018). Mesenchymal stem cell-derived extracellular vesicles: novel frontiers in regenerative medicine. Stem Cell Res. Ther. *9*, 63. https://doi.org/10.1186/s13287-018-0791-7.

22. Jones, J.I., and Clemmons, D.R. (1995). Insulin-like growth factors and their binding proteins: biological actions. Endocr. Rev. *16*, 3–34. https://doi.org/10.1210/edrv-16-1-3.

23. Ansari, K.I., Bhan, A., Liu, X., Chen, M.Y., and Jandial, R. (2020). Astrocytic IGFBP2 and CHI3L1 in cerebrospinal fluid drive cortical metastasis of HER2+breast cancer. Clin. Exp. Metastasis *37*, 401–412. https://doi.org/10.1007/s10585-020-10032-4.

24. Sun, L., Zhang, X., Song, Q., Liu, L., Forbes, E., Tian, W., Zhang, Z., Kang, Y., Wang, H., Fleming, J.B., et al. (2021). IGFBP2 promotes tumor progression by inducing alternative polarization of macrophages in pancreatic ductal adenocarcinoma through the STAT3 pathway. Cancer Lett. *500*, 132–146. https://doi.org/10.1016/j.canlet.2020.12.008.

25. Guo, Q., Yu, D.Y., Yang, Z.F., Liu, D.Y., Cao, H.Q., and Liao, X.W. (2020). IGFBP2 upregulates ZEB1 expression and promotes hepatocellular carcinoma progression through NF-kappaB signaling pathway. Dig. Liver Dis. *52*, 573–581. https://doi.org/10.1016/j.dld.2019.10.008.

26. Wang, F., Zhang, L., Sai, B., Wang, L., Zhang, X., Zheng, L., Tang, J., Li, G., and Xiang, J. (2020). BMSC-derived leptin and IGFBP2 promote erlotinib resistance in lung adenocarcinoma cells through IGF-1R activation in hypoxic environment. Cancer Biol. Ther. *21*, 61–71. https://doi.org/10.1080/15384047.2019.1665952.

27. Weiner, T.M., Liu, E.T., Craven, R.J., and Cance, W.G. (1993). Expression of focal adhesion kinase gene and invasive cancer. Lancet *342*, 1024–1025. https://doi.org/10.1016/0140-6736(93)92881-s.

28. Murphy, J.M., Jeong, K., Rodriguez, Y.A.R., Kim, J.H., Ahn, E.Y.E., and Lim, S.T.S. (2019). FAK and Pyk2 activity promote TNF-alpha and IL-1beta-mediated pro-inflammatory gene expression and vascular inflammation. Sci. Rep. *9*, 7617. https://doi.org/10.1038/s41598-019-44098-2.

29. Li, C., Liu, Y., Li, Y., Tai, R., Sun, Z., Wu, Q., Liu, Y., and Sun, C. (2021). Collagen XV promotes ER stress-induced inflammation through activating integrin beta1/FAK signaling pathway and M1 macrophage polarization in adipose tissue. Int. J. Mol. Sci. *22*, 9997. https://doi.org/10.3390/ijms22189997.

30. Avizienyte, E., and Frame, M.C. (2005). Src and FAK signalling controls adhesion fate and the epithelial-to-mesenchymal transition. Curr. Opin. Cell Biol. *17*, 542–547. https://doi.org/10.1016/j.ceb.2005.08.007.

31. Yan, R., Wang, Y., Shi, M., Xiao, Y., Liu, L., Liu, L., and Guo, B. (2019). Regulation of PTEN/AKT/FAK pathways by PPARgamma impacts on fibrosis in diabetic nephropathy. J. Cell. Biochem. *120*, 6998–7014. https://doi.org/10.1002/jcb.27937.

32. Liu, Y., Li, F., Yang, Y.T., Xu, X.D., Chen, J.S., Chen, T.L., Chen, H.J., Zhu, Y.B., Lin, J.Y., Li, Y., et al. (2019). IGFBP2 promotes vasculogenic mimicry formation via regulating CD144 and MMP2 expression in glioma. Oncogene *38*, 1815–1831. https://doi.org/10.1038/s41388-018-0525-4.

33. Ma, Y., Cui, D., Zhang, Y., Han, C.C., and Wei, W. (2020). Insulin-like growth factor binding protein-2 promotes proliferation and predicts poor prognosis in hepatocellular carcinoma. OncoTargets Ther. *13*, 5083–5092. https://doi.org/10.2147/OTT.S249527.

34. Martens, K., Seys, S.F., Alpizar, Y.A., Schrijvers, R., Bullens, D.M.A., Breynaert, C., Lebeer, S., and Steelant, B. (2021). Staphylococcus aureus enterotoxin B disrupts nasal epithelial barrier integrity. Clin. Exp. Allergy *51*, 87–98. https://doi.org/10.1111/cea.13760.

35. Murphy, J., Ramezanpour, M., Roscioli, E., Psaltis, A.J., Wormald, P.J., and Vreugde, S. (2018). Mucosal zinc deficiency in chronic rhinosinusitis with nasal polyposis contributes to barrier disruption and decreases ZO-1. Allergy *73*, 2095–2097. https://doi.org/10.1111/all.13532.

36. Li, X., Li, C., Zhu, G., Yuan, W., and Xiao, Z.A. (2019). TGF-beta1 induces epithelial-mesenchymal transition of chronic sinusitis with nasal polyps through MicroRNA-21. Int. Arch. Allergy Immunol. *179*, 304–319. https://doi.org/10.1159/000497829.

37. Zhao, M., Liu, S., Wang, C., Wang, Y., Wan, M., Liu, F., Gong, M., Yuan, Y., Chen, Y., Cheng, J., et al. (2021). Mesenchymal stem cell-derived extracellular vesicles attenuate mitochondrial damage and inflammation by stabilizing mitochondrial DNA. ACS Nano *15*, 1519–1538. https://doi.org/10.1021/acsnano.0c08947.

38. Ge, X., Meng, Q., Wei, L., Liu, J., Li, M., Liang, X., Lin, F., Zhang, Y., Li, Y., Liu, Z., et al. (2021). Myocardial ischemia-reperfusion induced cardiac extracellular vesicles harbour proinflammatory features and aggravate

heart injury. J. Extracell. Vesicles *10*, e12072. https://doi.org/10.1002/jev2.12072.

39. Vizoso, F.J., Eiro, N., Cid, S., Schneider, J., and Perez-Fernandez, R. (2017). Mesenchymal stem cell secretome: toward cell-free therapeutic strategies in regenerative medicine. Int. J. Mol. Sci. *18*, 1852. https://doi.org/10.3390/ijms18091852.

40. Harman, R.M., Marx, C., and Van de Walle, G.R. (2021). Translational animal models provide insight into mesenchymal stromal cell (MSC) secretome therapy. Front. Cell Dev. Biol. *9*, 654885. https://doi.org/10.3389/fcell.2021.654885.

41. Liu, C.H., and Hwang, S.M. (2005). Cytokine interactions in mesenchymal stem cells from cord blood. Cytokine *32*, 270–279. https://doi.org/10.1016/j.cyto.2005.11.003.

42. Gnecchi, M., Danieli, P., Malpasso, G., and Ciuffreda, M.C. (2016). Paracrine mechanisms of mesenchymal stem cells in tissue repair. Methods Mol. Biol. *1416*, 123–146. https://doi.org/10.1007/978-1-4939-3584-0_7.

43. Ferrari, G., Cook, B.D., Terushkin, V., Pintucci, G., and Mignatti, P. (2009). Transforming growth factor-beta 1 (TGF-beta1) induces angiogenesis through vascular endothelial growth factor (VEGF)-mediated apoptosis. J. Cell. Physiol. *219*, 449–458. https://doi.org/10.1002/jcp.21706.

44. Cho, S.H., Kim, D.W., and Gevaert, P. (2016). Chronic rhinosinusitis without nasal polyps. J. Allergy Clin. Immunol. Pract. *4*, 575–582. https://doi.org/10.1016/j.jaip.2016.04.015.

45. Huang, B.R., Bau, D.T., Chen, T.S., Chuang, I.C., Tsai, C.F., Chang, P.C., Hsu, H.C., and Lu, D.Y. (2018). Pro-inflammatory stimuli influence expression of intercellular adhesion molecule 1 in human anulus fibrosus cells through FAK/ERK/GSK3 and PKCdelta signaling pathways. Int. J. Mol. Sci. *20*, 77. https://doi.org/10.3390/ijms20010077.

46. Maxson, M.E., Naj, X., O'Meara, T.R., Plumb, J.D., Cowen, L.E., and Grinstein, S. (2018). Integrin-based diffusion barrier separates membrane domains enabling the formation of microbiostatic frustrated phagosomes. Elife *7*, e34798. https://doi.org/10.7554/eLife.34798.

47. Zhang, N., Van Crombruggen, K., Gevaert, E., and Bachert, C. (2016). Barrier function of the nasal mucosa in health and type-2 biased airway diseases. Allergy *71*, 295–307. https://doi.org/10.1111/all.12809.

48. Gao, Y.B., Zhang, Y., and Zhang, L. (2019). [Advance in epithelial-mesenchymal transition in chronic rhinosinusitis]. Zhonghua er bi yan hou tou jing wai ke za zhi *54*, 231–236. https://doi.org/10.3760/cma.j.issn.1673-0860.2019.03.015.

49. Gan, W., Zhang, H., Yang, F., Liu, S., Liu, F., and Meng, J. (2021). The influence of nasal microbiome diversity and inflammatory patterns on the prognosis of nasal polyps. Sci. Rep. *11*, 6364. https://doi.org/10.1038/s41598-021-85292-5.

50. Chiarella, E., Lombardo, N., Lobello, N., Piazzetta, G.L., Morrone, H.L., Mesuraca, M., and Bond, H.M. (2020). Deficit in adipose differentiation in mesenchymal stem cells derived from chronic rhinosinusitis nasal polyps compared to nasal mucosal tissue. Int. J. Mol. Sci. *21*, 9214. https://doi.org/10.3390/ijms21239214.

51. Shojaati, G., Khandaker, I., Funderburgh, M.L., Mann, M.M., Basu, R., Stolz, D.B., Geary, M.L., Dos Santos, A., Deng, S.X., and Funderburgh, J.L. (2019). Mesenchymal stem cells reduce corneal fibrosis and inflammation via extracellular vesicle-mediated delivery of miRNA. Stem Cells Transl. Med. *8*, 1192–1201. https://doi.org/10.1002/sctm.18-0297.

52. Yao, X., Wang, Y., Duan, Y., Zhang, Q., Li, P., Jin, R., Tao, Y., Zhang, W., Wang, X., Jing, C., and Zhou, X. (2018). IGFBP2 promotes salivary adenoid cystic carcinoma metastasis by activating the NF-kappaB/ZEB1 signaling pathway. Cancer Lett. *432*, 38–46. https://doi.org/10.1016/j.canlet.2018.06.008.

53. Ding, S.M., Lu, A.L., Lu, J.F., Chen, X.L., Edoo, M.I.A., Zhou, L., Xie, H.Y., Zheng, S.S., and Li, Q.Y. (2020). Macrovascular endothelial cells enhance the motility of liver cancer cells by up-regulation of MMP-3, activation of integrin/FAK signaling pathway and induction of non-classical epithelial-mesenchymal transition. J. Cancer *11*, 2044–2059. https://doi.org/10.7150/jca.38209.

54. Alam, S.K., Yadav, V.K., Bajaj, S., Datta, A., Dutta, S.K., Bhattacharyya, M., Bhattacharya, S., Debnath, S., Roy, S., Boardman, L.A., et al. (2016). DNA damage-induced ephrin-B2 reverse signaling promotes chemoresistance and drives EMT in colorectal carcinoma harboring mutant p53. Cell Death Differ. *23*, 707–722. https://doi.org/10.1038/cdd.2015.133.

55. Hara, S., Tojima, I., Shimizu, S., Kouzaki, H., and Shimizu, T. (2022). 17, 18-epoxyeicosatetraenoic acid inhibits TNF-alpha-induced inflammation in cultured human airway epithelium and LPS-induced murine airway inflammation. Am. J. Rhinol. Allergy *36*, 106–114. https://doi.org/10.1177/19458924211027682.

56. Jaiswal, A., Dash, D., and Singh, R. (2022). Intranasal curcumin and dexamethasone combination ameliorates inflammasome (NLRP3) activation in lipopolysachharide exposed asthma exacerbations. Toxicol. Appl. Pharmacol. *436*, 115861. https://doi.org/10.1016/j.taap.2021.115861.

57. Krammer, S., Yang, Z., Zimmermann, T., Xepapadaki, P., Geppert, C.I., Papadopoulos, N.G., and Finotto, S. (2022). An immunoregulatory role of interleukin-3 in allergic asthma. Front. Immunol. *13*, 821658. https://doi.org/10.3389/fimmu.2022.821658.

58. Ip, S., Ms, S., Av, K., Aa, N., Ed, B., Vi, K., Li, V., Vn, T., Kv, Y., Mm, K., et al. (2022). The mixture of siRNAs targeted to IL-4 and IL-13 genes effectively reduces the airway hyperreactivity and allergic inflammation in a mouse model of asthma. Int. Immunopharmacol. *103*, 108432. https://doi.org/10.1016/j.intimp.2021.108432.

59. Lee, M., Kim, D.W., Yoon, H., So, D., Khalmuratova, R., Rhee, C.S., Park, J.W., and Shin, H.W. (2016). Sirtuin 1 attenuates nasal polypogenesis by suppressing epithelial-to-mesenchymal transition. J. Allergy Clin. Immunol. *137*, 87–98.e7. https://doi.org/10.1016/j.jaci.2015.07.026.

60. Shin, H.W., Cho, K., Kim, D.W., Han, D.H., Khalmuratova, R., Kim, S.W., Jeon, S.Y., Min, Y.G., Lee, C.H., Rhee, C.S., and Park, J.W. (2012). Hypoxia-inducible factor 1 mediates nasal polypogenesis by inducing epithelial-to-mesenchymal transition. Am. J. Respir. Crit. Care Med. *185*, 944–954. https://doi.org/10.1164/rccm.201109-1706OC.

STAR★METHODS

KEY RESOURCES TABLE

REAGENT or RESOURCE	SOURCE	IDENTIFIER (DILUTION)
Antibodies		
IGFBP2	Proteintech	11065-3-AP (WB, 1:500; IHC, 1:200)
IGFBP2	Abcam	ab188200 (IF, 1:300)
ZO-1	Proteintech	66452-1-Ig (WB, 1:500; IHC, 1:200)
E-cadherin	Cell Signaling Technology	14472S (WB, 1:1000; IHC, 1:200; IF,1:100)
N-cadherin	Cell Signaling Technology	13116T (WB, 1:1000; IHC, 1:150; IF,1:100)
Vimentin	Cell Signaling Technology	5741T (WB, 1:1000; IHC, 1:200; IF,1:100)
TGF-β1	Proteintech	21898-1-AP (WB, 1:500; IHC, 1:200; IF,1:200)
GAPDH	Proteintech	10494-1-AP (1:500)
Occludin	Proteintech	27260-1-AP (WB, 1:500; IHC, 1:2000; IF,1:500)
Claudin-1	Proteintech	28674-1-AP (WB, 1:500; IHC, 1:200; IF,1:200)
CD73	Fcmacs Biotech Co	12-0739-41
CD90	Fcmacs Biotech Co	12-0909-41
CD105	Fcmacs Biotech Co	12-1057-41
CD34	Fcmacs Biotech Co	12-0349-41
CD45	Fcmacs Biotech Co	12-0459-41
HLA-DR	Fcmacs Biotech Co	12-9956-41
IgG	Fcmacs Biotech Co	12-4714-82
ALIX	Abcam	ab275377 (WB,1:1000)
TSG101	Abcam	ab125011 (WB,1:1000)
CD9	Abcam	ab236630 (WB,1:1000)
CD63	Proteintech	25682-1-AP (WB,1:1000)
Actinin-4	Abcam	ab108198 (WB,1:1000)
Albumin	Abcam	ab207327 (WB,1:1000)
Flotillin-1	Abcam	ab133497 (WB,1:1000)
MMP9	Cell Signaling Technology	13667T (WB,1:1000)
MCP-1	Proteintech	66272-1-Ig (WB, 1:500)
VEGFA	Proteintech	66828-1-Ig (WB, 1:500)
IL-1β	Cell Signaling Technology	12703S (WB,1:1000)
p-FAK	Cell Signaling Technology	D20B1 (WB,1:1000)
t-FAK	Cell Signaling Technology	71433T (WB,1:1000)
p-MEK1/2	Cell Signaling Technology	2338S (WB,1:1000)
t-MEK1/2	Cell Signaling Technology	8727T (WB,1:1000)
CK7	Cell Signaling Technology	4465T (IF,1:200)
MBP	Cell Signaling Technology	78896T (IF,1:100)
α-SMA	Cell Signaling Technology	19245T (IF,1:200)
MPO	Proteintech	6617-1-Ig (IF,1:200)
CY3-TSA	Servicebio	G1223
FITC-TSA	Servicebio	G1222
CY5	Servicebio	GB27303
Bacterial and virus strains		
Synthetic IGFBP2 si-RNA	Shanghai Genechem	Target seq: ACAGCACCATGAACATGTT

(*Continued on next page*)

Continued

REAGENT or RESOURCE	SOURCE	IDENTIFIER (DILUTION)
Synthetic TGF-β1 si-RNA	Shanghai Genechem	Target seq: CACTGCAAGTGGACATCAA
Biological samples		
Mouse tissues	This paper	N/A
Human IT and NP specimens	Affiliated Hospital of Nantong University	N/A
Chemicals, peptides, and recombinant proteins		
DMSO	Thermo Fisher Scientific	Cat#BP231-100
TGF-β1	PeproTech	AF-100-21C
Proteinase K	YEASEN	10401ES60
GW4869	Bromisoval	6823-69-4
Alexa Fluor-conjugated secondary antibodies	Invitrogen	1832039
Hochest	Thermo Fisher Scientific	62249
DAPI	Sigma	D9542
Fetal Bovine Serum	Biological Industries	04-001-1ACS
DMEM	Biological Industries	C3133-P050K
BEGM	Promo Cell	C21060
TRIzol reagent	BBI	B511311
fluorescein isothiocyanate–dextran 4kDa	Thermo Fisher Scientific	D1844
Critical commercial assays		
RIPA Lysis and Extraction Buffer	Thermo Fisher Scientific	89900
BCA protein assay kit	Pierce	23227
SYBR Green PCR Master Mix	Biosystems	00675137
Osteogenesis	Cyagen	HUXMA-90021
Adipogenic	Cyagen	HUXMA-90031
PKH-67 labeling kit	Sigma	PKH67GL
Oligonucleotides		
Primer1 for E-cadherin, Forward ATT GCT CAC ATT TCC CAA CTC C	This paper	N/A
Primer1 for E-cadherin, Reverse CTC TGT CAC CTT CAG CCA TCC	This paper	N/A
Primer1 for N-cadherin Forward ATC CTC CAG AGT TTA CTG CCA TG	This paper	N/A
Primer1 for N-cadherin, Reverse ACG GTG ACT AAC CCG TCG TT	This paper	N/A
Primer1 for Vimentin, Forward CCT TGA ACG CAA AGT GGA ATC	This paper	N/A
Primer1 for Vimentin, Reverse GTG AGG TCA GGC TTG GAA ACA	This paper	N/A
Primer1 for GAPDH, Forward ACA TCA AGA AGG TGG TGA AGC A	This paper	N/A
Primer1 for GAPDH, Reverse AAA GGT GGA GGA GTG GGT GTC	This paper	N/A
Primer1 for β-actin, Forward CAG CCA TGT ACG TTG CTA TC	This paper	N/A
Primer1 for β-actin, Reverse CAT GAG GTA GTC AGT CAG GT	This paper	N/A

(*Continued on next page*)

Continued

REAGENT or RESOURCE	SOURCE	IDENTIFIER (DILUTION)
Primer1 for RPLP0, Forward CAT TGA AAT CCT GGG TGT CCG	This paper	N/A
Primer1 for RPLP0, Reverse TTG ACC TTT TCA GCA AGT GGG	This paper	N/A
Primer1 for RPLP1, Forward AGC TCG CCT GCA TCT ACT CG	This paper	N/A
Primer1 for RPLP1, Reverse GCA TTG ATC TTA TCC TCC GTG A	This paper	N/A
Experimental models: Cells		
Human: pHNECs	This paper	N/A
MSCs	This paper	N/A
Software and algorithms		
GraphPad Prism	Graphpad Software	www.graphpad.com/scientific- software/ prism/
Image processing and analysis	ImageJ	https://imagej.nih.gov/ij/in Java

RESOURCE AVAILABILITY

Lead contact

Further information and requests for resources and reagents should be directed to and will be fulfilled by the lead contact, Jing Chen (chenjing0408@hotmail.com).

Materials availability

This study did not generate new unique reagents.

Data and code availability

Data: All data reported in this paper will be shared by the lead contact upon request.

Code: This paper does not report original code. Any additional information required to reanalyze the data in this paper is available upon request from the lead contact.

EXPERIMENTAL MODEL AND SUBJECT DETAILS

Human subjects

In total, 116 patients were recruited for this study. 80 patients with NPs diagnosed according to the European Position Paper on Rhinosinusitis and Nasal Polyps 2020 guidelines (EPOS 2020). Patients with ciliary dysfunction, cystic fibrosis, autoimmune disease, immunodeficiency, and history of sinus surgery were excluded. None of the patients had aspirin intolerance. During surgery, polyp tissues from NPs (36 female and 44 male, 43.3 $\pm$ 3.93 years old), and inferior turbinate tissues from control subjects (16 female and 20 male, 41.75 $\pm$ 3.93 years old) were collected.

This study was approved by the Human Ethics Committee of the Nantong University Affiliated Hospital, and all patients provided written informed consent for participation in the study. This study followed the principles guidelines of the Declaration of Helsinki. Additional patient details are described in Table 1.

Experimental animals BALB/c mice

BALB/c male mice (5-week-old, average weight 20g) were obtained from Laboratory Animal Center of Nantong University, and raised in specific pathogen-free rooms, and maintained conditions were comparable between all treatments and controls between all groups. All experimental protocols complied with the Guidelines of the National Institute of Health and the Declaration of Helsinki and were approved by the Committee on the Use and Care of Animals (No. S20220301-040).

The model-building process consists of two stages: the sensitization stage and challenged stage, but we made some modifications. First, we took TGF-β1 as the positive control and set the IGFBP2 concentration gradients (4ug/kg and 20ug/kg) referent to the literature,[55–58] we opted for the latter. Mice were divided into 5 groups (n = 5; either sex): Control, TGF-β1, 4ug/kg IGFBP2, 20ug/kg IGFBP2 and 20ug/kg IGFBP2 + PF573228. To sensitize the mice, intraperitoneal injection (i.p.) of 200 μl PBS containing ovalbumin (OVA, 100 μg) emulsified in alum (2 mg). Simultaneously, intranasal instillation (i.n.) of 100 μl mixture combinations of OVA (50 μg) and *Aspergillus oryzae* (AP, 2 U) for 7 consecutive days. Then, intranasal instillation 100 μl PBS mixture dissolved OVA, AP and different stimulus on 14 consecutive days from 8 to 21 to challenge the mice. Following 21 days treatments, mice were sacrificed after anesthesia and collected the sinonasal specimens to measure the nasal epithelial EMT and barrier function of different groups. EMT and epithelial disruption were microscopically examined from three coronal sections. The criteria included (1) the expression of epithelial and mesenchymal phenotype, (2) more elevated lesion than surrounding mucosal folds, and (3) eosinophilic infiltration.[59,60]

METHOD DETAILS

Cells culture, stimulation and transfection

Primary human nasal epithelial cells (pHNECs) were isolated using an enzymatic method. The obtained specimens of human healthy mucosa were rinsed recurrently and digested with Proteinase K (YEASEN, China) in serum-free medium DMEM to further prepare suspensions. Then, cell pellets were resuspended in serum-free Airway Epithelial Cell Growth-Medium (BEGM, PromoCell, Germany) and cultured under the condition with 95% humidified air and 5% CO_2 at 37°C. After pHNECs reached about 80% confluency, they were changed to air-liquid interface (ALI) culture.

For MSCs purification and culture. Single-cell suspensions were prepared by enzymatic digestion of inferior turbinate and NPs tissues. Simultaneously, suspensions incubation with anti-CD45 and anti-epithelial cell adhesion molecule (EpCAM) magnetic beads (Miltenyi Biotech), and then passage through a magnetic column for negative sorting. Subsequently, the bead-negative population were cultured separately at 37°C with 5% CO_2 in complete MesenCult™-ACF Plus Medium (STEMCELL Technologies, China). Trypan blue exclusion was utilized to assess the viability, and finally calculated the purity and yield of sorted cells. Fresh medium was replaced every 2–3 days. After reaching 70% confluence and incubated for 48 h to collect conditioned medium (CM). Moreover, once a uniform monolayer of adherent cells is reached, PO-MSCs were treated with GW4869[38] (an inhibitor for EVs release) for 48 h and then collected CM for subsequent experiments. All experiments were performed with MSCs at passage 3 or 4.

For construction of the EMT cells model, pHNECs were treated with 10 ng/mL human recombinant transforming growth factor-β1 (TGF-β1, PeproTech, USA) for 48 h.

For PO-MSCs and pHNECs siRNA transfection experiments, synthetic IGFBP2 siRNA, TGF-β1 siRNA and their corresponding controls were obtained from Genechem (Shanghai, China). Lipofectamine 2000 (Invitrogen, USA) was used in siRNAs transfection. After 72 h, qRT-PCR or western blot were performed to verify transfection efficiency. The cells were harvested and utilized for subsequent experiments.

Histology and immunohistochemistry

Histology and immunohistochemistry were performed to verify the expression levels of E-cadherin, Vimentin, N-cadherin, TGF-β1 and zona occludens-1 (ZO-1) in tissue specimens. The following antibodies were used: anti-E-cadherin (CST, USA), anti-N-cadherin (CST, USA), anti-Vimentin (CST, USA), anti- TGF-β1 (CST, USA) and anti-ZO-1 (Proteintech, China).

Immunofluorescence and triple fluorescence staining

pHNECs were fixed with 4% paraformaldehyde at room temperature for 20 min. Thereafter, cells were blocked with 5% bovine serum albumin for 1 h, incubated with antibodies at 4 °C overnight, incubated with Alexa Fluor-conjugated secondary antibodies (Invitrogen, USA), and counterstained with DAPI (Sigma, USA). Fluorescent images were acquired using a fluorescence microscope.

For triple fluorescence staining, tissue sections were deparaffinized, rehydrate and incubated with citrate buffer for antigen retrieval. Then, immersed sections in 3% and incubated to block endogenous

peroxidase. Sections were incubated with primary antibody, followed by incubation with HRP-labeled secondary antibody in Rocker device. Afterwards, the slides were immersed in CY3-TSA (Servicebio, G1222, China) and FITC-TSA (Servicebio, G1223, China) solutions and incubated with the second primary antibody and the third primary antibody and their corresponding secondary antibodies, respectively. The third corresponding secondary antibody was marked with CY5 (Servicebio, G1223, China). After counterstaining the nucleus with DAPI and quenching the fluorescence, the slice scanner was used to detect and collect images. DAPI glows blue by UV excitation wavelength 330–380 nm and emission wavelength 420 nm; FITC glows green by excitation wavelength 465–495 nm and emission wavelength 515–555 nm; CY3 glows red by excitation wavelength 510–560 nm and emission wavelength 590 nm. CY5 glows pink by excitation wavelength 608-648 nm and emission wavelength 672-712nm. (CY5 was originally red, in order to distinguish it from CY3, we set it to pink light.) The primary antibodies as following: anti-ZO-1 (Proteintech, China), anti-Occludin (Proteintech, China), anti-IGFBP2 (Proteintech, China), anti-CD105 (CST, USA), anti-CD90 (CST, USA), anti-CD73 (CST, USA), anti-TGF-β1 (CST, USA), anti-CK7 (CST, USA), anti-MPO (Proteintech, China), anti-MBP (CST, USA) and anti-α-SMA (CST, USA).

Western blot analysis

Briefly, total protein was extracted using RIPA lysis buffer containing protease inhibitor, phenylmethylsulfonyl fluoride and phosphatase. BCA protein assay kit (Pierce, USA) was used to measure protein concentrations in samples. Approximately 10 μg protein was separated using sodium dodecyl sulfatepolyacrylamide gel electrophoresis. Proteins were then transferred to polyvinylidene difluoride membranes (Millipore; cat. no. ISEQ00010, USA). The membranes were incubated with the following primary antibodies: anti-E-cadherin (CST, USA), anti-Vimentin (CST, USA), anti-N-cadherin (CST, USA), anti-TGF-β1(CST, USA), anti-ZO-1(Proteintech, China), anti-IGFBP2 (Proteintech, China), anti-Occludin (Proteintech, China), anti-Claudin-1 (Proteintech, China), anti-FAK (CST, USA), anti-MEK1/2 (CST, USA), and anti-glyceraldehyde 3-phosphate dehydrogenase (GAPDH; Proteintech, China). ImageJ software was used for quantification.

Reverse transcription quantitative polymerase chain reaction (RT-qPCR)

pHENCs total RNA was extracted using TRIzol reagent (Invitrogen, USA) and then reverse transcribed into cDNA. qPCR amplification was conducted using SYBR Green PCR Master Mix (Biosystems, USA) to detect mRNA expression levels. The relative gene expression was calculated by the change-in-threshold $2^{-\Delta CT}$ method. GAPDH served as endogenous control for normalization.

Epithelial permeability assay

To assess epithelial permeability, a surrogate marker of layer integrity was measured by using fluorescein isothiocyanate–dextran 4 kDa (Thermo, USA). pHNECs were seeded into 0.4 μm Transwell chambers (Costar, USA) in 24-well plates. After cells reached confluence, fluorescein isothiocyanate-dextran (1 mg/mL) was added to the upper chamber in ALI culture. Fifty microliters sample was collected from the lower chamber at different time points, and a fluorescence plate reader (Lambda Fluoro 320; Germany) was used to measure the optical density value to quantify permeability changes.

Wound-healing assay

pHNECs were plated into six-well plates and performed different treatment for 48 h. Next, the confluent cell layer was scratched and rinsed with phosphate-buffered saline (PBS), and then the fresh medium was replaced. The area of wound healed was monitored, and representative wounds were photographed using an optical microscope (Zeiss, Jena, Germany).

Flow cytometry

Single-cell suspensions of PO-MSCs were incubated with anti-CD73, anti-CD90, anti-CD105, anti-CD34, anti-CD45, and anti-HLA-DR antibodies in the dark. All antibodies were purchased from Fcmacs Biotech Co (China). PO-MSCs were washed and resuspended in PBS, and then detected using a flow cytometer. Propidium iodide (Sigma-Aldrich, Germany) was used to eliminate dead cells and debris. All data were analyzed by FlowJo software (FlowJo).

Osteogenesis and adipogenic differentiation

To evaluate the multipotential differentiation, third-passage PO-MSCs were seeded in six-well plates and cultured at a density of 2×10^5 cells per well. After the PO-MSCs reached about 80% confluence, their culture medium was changed to osteogenesis differentiation medium or adipogenic differentiation medium (all from Cyagen, Guangzhou, China) and induction 21 days according to the manufacturer's protocol, respectively. Then, Oil Red staining and Alizarin Red S staining were subjected to verify the adipogenic differentiation and osteogenic differentiation, respectively.

Isolation and identification of extracellular vesicles (EVs)

In short, supernatants were conducted differential centrifugation to remove the cell debris. Then, 0.2-μm filter (Sarstedt, Germany) and qEV size-exclusion columns (iZON Science, Christchurch, New Zealand) were utilized to further purification. Subsequently, the supernatant was ultracentrifuged (Type 90 Ti rotor; Beckman Coulter, CA, USA) at 100,000 × g for 60 minat 4°C to generate EVs pellets. Finally, the pellets were washed once with PBS and frozen at −80°C for further experiments.

For identification of EVs, western blot analysis showed that the EVs specific markers (ALIX, TSG101, CD9, CD63 and Flotillin-1) were highly enriched in EVs derived from PO-MSCs. The primary antibodies we used were: anti-CD9 antibody (Abcam, USA), anti-CD63 antibody (Proteintech, China), anti-TSG101 antibody (Abcam, USA), anti-ALIX antibody (Abcam, USA), anti-Flotillin-1 antibody (Abcam, USA), anti-actinin-4 antibody (Abcam, USA) and anti-albumin antibody (Abcam, USA). Transmission Electron Microscope (JEM-1230; JEOL, Ltd., Tokyo, Japan) was utilized to observe the morphology of EVs. Uptake experiments were performed with a PKH-67 labeling kit (Sigma, USA) for labeling EVs to observe cellular uptake of EVs.

Cell culture and ELISA aassay

Neutrophils (BFN-60804794) and eosinophils (BFN-607200671) were purchased from BFB company (China). Fibroblasts (KCB 200537) were obtained from Cell Bank of Typical Culture Preservation Commission, Chinese academy of Sciences.

TGF-β1 and IGFBP2 in the cells supernatant were determined via an enzyme-linked immunosorbent assay (ELISA) by available ELISA sets (ExCellBio and Elabscience, China) in accordance with the manufacturer's instructions. Optical densities were measured in an ELISA platereader at 450-nm wave length. All samples were measured in triplicate.

QUANTIFICATION AND STATISTICAL ANALYSIS

Statistical analysis was performed using GraphPad Prism and SPSS software (IBM Corp.,USA). All data were expressed as means ± standard deviations from at least three independent experiments. Student's t-tests and one-way analysis of variance were applied to determine statistical significance. Qualitative variables were evaluated using Fisher exact tests. Correlation analysis was performed using Spearman and Pearson correlation analyses. Results with p values less than 0.05 were considered statistically significant.